Available online at www.sciencedirect.com

ScienceDirect

Geochimica et Cosmochimica Acta 129 (2014) 125–145

Geochimica et Cosmochimica Acta

www.elsevier.com/locate/gca

Water in the deep Earth: The dielectric constant and the solubilities of quartz and corundum to 60 kb and 1200 °C

Dimitri A. Sverjensky [a,b,*], Brandon Harrison [a], David Azzolini [a]

[a] Department of Earth & Planetary Sciences, Johns Hopkins University, Baltimore, MD 21218, United States
[b] Geophysical Laboratory, Carnegie Institution of Washington, Washington, DC 20015, United States

Received 23 July 2013; accepted in revised form 1 December 2013; Available online 31 December 2013

Abstract

Comprehensive quantitative theoretical evaluation of water–rock interactions in the Earth has long been restricted to a pressure of 5.0 kb – too low to address processes involving deep aqueous fluids. Yet such fluids are thought to play an important role in the long-term geologic cycling of many chemical elements. A reason for this restriction is the lack of information on the dielectric constant of water (ε_{H_2O}) needed for the revised Helgeson–Kirkham–Flowers (HKF) equations of state for aqueous species. Equation of state coefficients are available for hundreds of aqueous species in SUPCRT92, but calculations using these species can only be made to 5.0 kb (Shock et al., 1992).

In the present study, the applicability of the revised HKF equations of state for aqueous species was extended to 60 kb by developing estimates of (ε_{H_2O}). We used a statistical mechanically-based equation for the dielectric constant of a hard-sphere fluid applicable to water (Franck et al., 1990). The equation was calibrated with experimental data, and data from a comprehensive analysis of the literature (Fernández et al., 1997), and then used to calculate (ε_{H_2O}) to a density of 1.1 g cm^{-3}. The values of $\ln(\varepsilon_{H_2O})$ were found to be linear with $\ln(\rho_{H_2O})$ which enabled empirical extrapolation of (ε_{H_2O}) to 60 kb. Values of ρ_{H_2O} were computed with a recent comprehensive evaluation consistent with experimental data and a molecular dynamics model for water (Zhang and Duan, 2005).

The resulting dielectric constants were tested at 727 °C and 58 kb by comparison with the results of *ab initio* molecular dynamics calculations (Pan et al., 2013). Additional testing was carried out by computing standard Gibbs free energies of aqueous species using the new values of (ε_{H_2O}) and ρ_{H_2O} in the revised HKF equations to predict equilibrium constants which in turn enabled calculation of the solubilities of quartz and corundum for comparison with experimental measurements to 20 kb and 1100 °C. Our results strongly suggest that geochemically useful predictions can now be made that will facilitate analysis of water–rock interactions in the Earth at depths much greater than previously possible.

1. INTRODUCTION

Aqueous geochemical calculations have long been used to quantitatively model the chemistry of water–rock interactions in hydrothermal systems in the Earth's crust (Helgeson, 1964, 1970, 1979; Sverjensky, 1987; Bethke, 1996; McCollom and Shock, 1998; Zhu and Anderson, 2002; Manning, 2004; Anderson, 2005; Dolejš and Manning, 2010; Shock and Canovas, 2010; Dolejš, 2013; Pokrovski et al., 2013). Such calculations rely on equilibrium constants involving minerals and aqueous species at elevated temperatures and pressures. Owing to the inherent chemical complexities of natural systems, the successful application of geochemical models of water–rock interaction requires data files containing equilibrium constants

* Corresponding author at: Department of Earth & Planetary Sciences, Johns Hopkins University, Baltimore, MD 21218, United States. Tel.: +1 4105168568.
E-mail address: sver@jhu.edu (D.A. Sverjensky).

0016-7037/$ - see front matter © 2014 Elsevier Ltd. All rights reserved.
http://dx.doi.org/10.1016/j.gca.2013.12.019

for a very wide range of aqueous species and minerals. However, because of the paucity of experimental data, integrated experimental and theoretically-based predictive approaches are essential to generating the equilibrium constants necessary for studying natural systems.

One approach to predicting equilibrium constants involving aqueous species involves correlating the logarithms of experimentally derived equilibrium constants, or solubilities, with the logarithm of the density of water. The coefficients in the correlations range from being completely empirical (Marshall and Franck, 1981; Manning, 1994; Marshall, 2008) to being thermodynamically calculable (Anderson et al., 1991; Dolejš and Manning, 2010). This approach is well-suited to providing estimates of equilibrium constants of individual reactions involving aqueous species only or individual mineral solubilities. However, it is not well-suited for the prediction of large data files involving many individually predicted mineral solubilities because of the difficulty in maintaining internal consistency with the results of independent phase equilibria that do not involve aqueous species. For example, simple dehydration equilibria involving minerals, and particularly solid–solid reactions, cannot accurately be modeled by combining individually extrapolated mineral solubility reactions involving aqueous species.

The most general and widely-used approach to predicting equilibrium constants was pioneered in the 1970s by Helgeson and co-workers (Helgeson and Kirkham, 1974a,b, 1976; Helgeson et al., 1981). Here, the focus was on calculating the standard Gibbs free energies of formation of individual aqueous species at elevated temperatures and pressures by building on knowledge of the standard partial molal derivative properties such as the volumes and heat capacities as functions of temperature and pressure. The Helgeson–Kirkham–Flowers (HKF) equations of state were subsequently revised (Tanger and Helgeson, 1988) and a comprehensive series of correlations were developed to estimate the equation of state coefficients and standard partial molal properties when experimental data are lacking (Shock and Helgeson, 1988, 1990; Shock et al., 1989). Together, the HKF equations of state and the predictive correlations constitute a model that has been widely applied over a range of upper crustal temperatures and pressures to all types of aqueous species including ions, dissolved gases, complexes, and dissolved organic molecules (Shock and Helgeson, 1988, 1990; Shock et al., 1989, 1997; Sverjensky et al., 1997; Amend and Helgeson, 1997a; Plyasunov and Shock, 2001; Dick et al., 2006; Larowe and Helgeson, 2006).

Two limitations to the applicability of the HKF equations of state for aqueous species exist. First, based on the availability of new experimental data, it is now clear that the form of the HKF equations is inadequate to simultaneously describe the large variations in standard partial molal volumes and heat capacities of electrically neutral aqueous molecules in low-density solutions near the critical point of water (Plyasunov and Shock, 2001; Dolejš, 2013). Nevertheless, because changes in the standard partial molal Gibbs free energies of aqueous species are calculated from integration of the changes in heat capacities and volumes, they are less sensitive to uncertainties in the latter properties (Helgeson et al., 1981). As a consequence, and also because of the broad predictive capabilities of the HKF equations of state, the overall model remains extremely useful, particularly for prediction of the standard Gibbs free energies of aqueous species (and therefore equilibrium constants) up to temperatures of 350 °C along the liquid–vapor saturation curve for water and at elevated temperatures at pressures greater than about 2 kb (Bethke, 1996; Shock and Canovas, 2010; Amend et al., 2013; Dick and Shock, 2013; Manning et al., 2013).

Second, application of the HKF equations of state has always been limited to a maximum of 5.0 kb in pressure (Helgeson and Kirkham, 1974a,b, 1976; Helgeson et al., 1981; Johnson et al., 1992; Shock et al., 1992). This limitation prevents the applicability of theoretical aqueous geochemical calculations to geologic processes in the deep continental crust and the upper mantle (Dolejš, 2013). The reason for the upper pressure limit is the lack of information on a fundamental property of water: the dielectric constant (ε_{H_2O}). The dielectric constant of water arises in the HKF equation of state for the Gibbs free energies of aqueous species through a term derived from an application of the Born equation for the solvation of aqueous species (Helgeson and Kirkham, 1976). However, experimental data for (ε_{H_2O}) at elevated temperatures are limited to 550 °C and 5.0 kb (Heger et al., 1980), as indicated in Fig. 1. These and other lower temperature and pressure data were the subject of a comprehensive study resulting in equations for (ε_{H_2O}) and its temperature and pressure derivatives and the associated Debye–Hückel parameters (Helgeson and Kirkham, 1974a,b).

Calculations at temperatures greater than 550 °C were first made by retrieving (ε_{H_2O}) from measurements of the solubility of quartz to 900 °C (McKenzie and Helgeson, 1984) and subsequently facilitated by making use of a predictive equation for (ε_{H_2O}) valid for $\rho_{H_2O} < 0.5\ g\ cm^{-3}$ (Pitzer, 1983). For example, calculations of the free energies of aqueous species to 1000 °C and 5 kb are part of the widely-used code SUPCRT92 (Johnson et al., 1992). In this code, (ε_{H_2O}) is calculated from an empirical equation as a function of temperature and the density of water (Johnson and Norton, 1991), which in turn was calculated using an IAPWS formulation (Haar et al., 1984). The latter has been superseded by a more recent IAPWS study (Wagner and Pruβ, 2002) recommended to 1000 °C and 10 kb, and other treatments of the density of water valid to much high temperatures and pressures (Zhang and Duan, 2005, 2009).

In recent years, no new measurements of (ε_{H_2O}) at elevated temperature and pressure have been reported. However, a number of advances have been made in studying the properties of water under these conditions (see review by Dolejš, 2013). An exhaustive survey of (ε_{H_2O}) and a broadly integrative equation of state for it, based on the Kirkwood equation, has enabled predictions to 600 °C and 12 kb (Fernández et al., 1995, 1997). Molecular dynamics methods have also been used to predict (ε_{H_2O}) to 1000 °C and 20 kb (Wasserman et al., 1995). Most recently, *ab initio* molecular dynamics (AIMD) calculations have resulted in

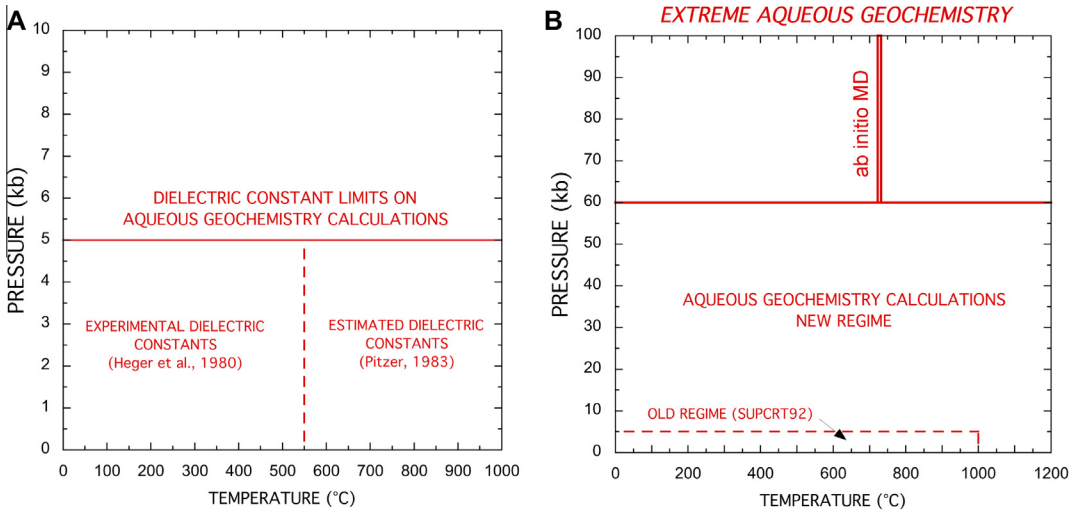

Fig. 1. High pressure and temperature limits on knowledge of the dielectric constant of water (ε_{H_2O}): (A) Traditional limits on (ε_{H_2O}) used in the HKF equations of state for the standard Gibbs free energies of aqueous species (see Johnson et al., 1992). (B) Expanded range for (ε_{H_2O}) in the present paper and in AIMD calculations of Pan et al. (2013).

the prediction of (ε_{H_2O}) at 727 and 1727 °C and three discrete pressures at 10, 58, 114 kb (Pan et al., 2013).

At the same time, dramatic advances have been made in measuring the solubilities of minerals in the pressure range 5–20 kb (Manning, 1994, 2013; Newton and Manning, 2000, 2002b, 2008; Dolejš and Manning, 2010; Newton et al., 2010; Manning et al., 2013) and in measuring *in situ* aqueous speciation to pressures as high as 70 kb (Frantz et al., 1994; Zotov and Keppler, 2000, 2002; Caciagli and Manning, 2003; Martinez et al., 2004; Chou et al., 2008; Mibe et al., 2008; Chou and Anderson, 2009; Mysen, 2009, 2010; Petitgirard et al., 2009; Mysen and Yamashita, 2010; Pokrovski and Dubrovinsky, 2011; Mysen et al., 2013a; Facq et al., 2014; Mysen et al., 2013b). Additional dramatic advances have also been made in measuring the densities of electrolyte solutions at unprecedented pressures (Mantegazzi et al., 2012, 2013; Sanchez-Valle, 2013). Taken together, the above studies emphasize the need for extension of the computational capabilities of the HKF equations to pressures above the long-standing limit of 5 kb.

In the present study, we report an extension of the HKF equations of state for the free energy of aqueous species to 60 kb and 1200 °C. We take advantage of a predictive equation for the dielectric constant at elevated pressures valid to $\rho_{H_2O} < 1.1$ g cm^{-3} (Franck et al., 1990). By calibration with experimental data from Heger et al. (1980) and Kirkwood equation predictions from Fernández et al. (1997), the Franck et al. equation can be extrapolated to much higher pressures than the 5 kb limit in SUPCRT92. For example, at 1000 °C the Franck equation can be used to about 25 kb. Beyond this pressure, we use an empirical correlation of the dielectric constant and the density of water, i.e. $\ln(\varepsilon_{H_2O})$ with $\ln(\rho_{H_2O})$, to extrapolate to 60 kb and 1200 °C. This approach is analogous to the use of the Kirkwood equation for extrapolations to high temperatures, but with the advantage that it can be tested at high pressures using recent AIMD results. The extensive measurements of mineral solubilities and aqueous speciation now available for elevated temperatures and pressures serve also as a test of the estimated dielectric constants, as well as the applicability of the HKF equations to extreme pressures.

2. DEVELOPMENT OF DIELECTRIC CONSTANT ESTIMATES AT HIGH PRESSURES

2.1. Equation of state for the density of water (ρ_{H_2O})

The densities of water used in the present study were calculated with a recent equation of state for water based on a comprehensive molecular dynamics study and calibrated with an extensive survey of experimental data (Zhang and Duan, 2005). This study was selected in preference to the IAPS formulation for water (Wagner and Pruß, 2002) that gives recommended values to only 10 kb. These values were used by Zhang and Duan (2005) in the development of their equation of state, together with a substantial amount of high pressure data for the density of water not considered in the IAPS formulation (Brodholt and Wood, 1994; Larrieu and Ayers, 1997; Withers et al., 2000; Abramson and Brown, 2004). Consequently, the equation of state for water used here is consistent with theory and experimental data referring to a very wide range of temperatures and pressures (Zhang and Duan, 2005). Although improvements have subsequently been made for pressures approaching 100 kb (Zhang and Duan, 2009), the treatment by Zhang and Duan (2005) was adopted in the present study because it is applicable to a geologically important continuum of low and high pressures.

For example, comparisons of the calculated values of the molar volume of water (VH_2O) with experimental data are illustrated in Fig. 2A–C. It can be seen in Fig. 2A that there is excellent agreement with experimental data referring to pressures of 1–8 kb (Burnham et al., 1969) and the equation of state from Zhang and Duan (2005). As these data were also previously used to constrain the equations in SUPCRT92, our use of Zhang and Duan (2005) ensures close agreement with the densities of water in SUPCRT92 for $P \geqslant 1.0$ kb. At much higher pressures, it can be seen

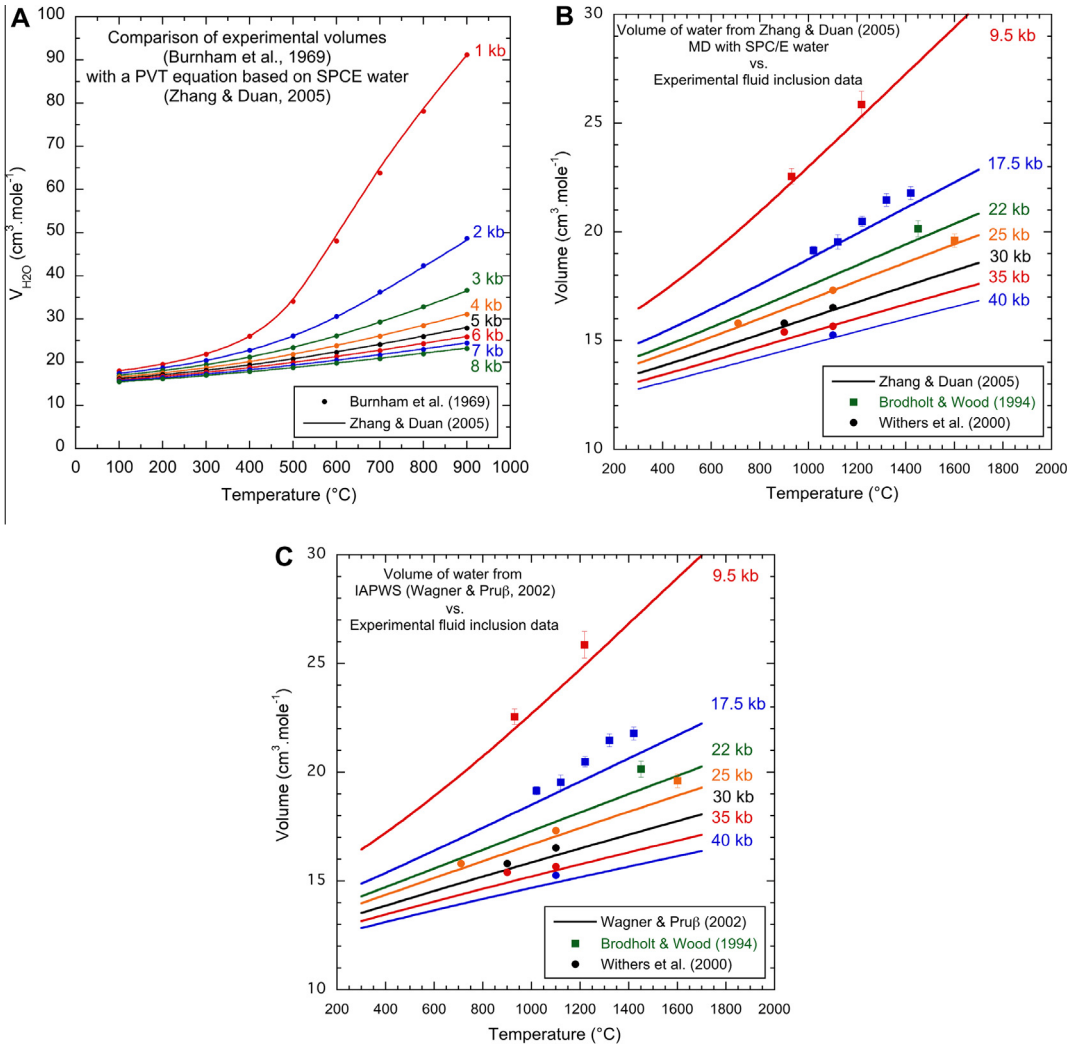

Fig. 2. Comparison of experimentally derived volumes of water with the equations of state from IAPWS (Wagner and Pruβ, 2002) and Zhang and Duan (2005). The equation state from Zhang and Duan (2005) fits the data better because the data were considered as part of the calibration over a very wide range of pressures and temperatures: (A) Points represent relatively low pressure experimental volumes of water from Burnham et al. (1969). Curves represent calculations from the equation of state. (B) Points represent high pressure experimental volumes of water from fluid inclusion studies by Brodholt and Wood (1994) and Withers et al. (2000). Curves represent calculations with the equation of state of Zhang and Duan (2005). (C) Points represent high pressure experimental volumes of water from fluid inclusion studies by Brodholt and Wood (1994) and Withers et al. (2000). Curves represent predictive extrapolations of the IAPWS equation of state (Wagner and Pruβ, 2002).

in Fig. 2B that overall good agreement exists with experimental fluid inclusion data (Brodholt and Wood, 1994; Withers et al., 2000) up to almost 1600 °C and 40 kb. Under this wide range of conditions, the treatment of Zhang and Duan (2005) is superior to other recent equations of state for water (Wagner and Pruβ, 2002; Zhang and Duan, 2009). Comparison of values predicted by extrapolation of the IAPWS formulation (Wagner and Pruβ, 2002) with the fluid inclusion data are shown in Fig. 2C. The calculated values are clearly not as accurate as those in Fig. 2B. The older IAPS formulation from Haar et al. (1984) used in SUPCRT92 up to 1000 °C performs very poorly at the pressures shown in Fig. 2B and C.

The upper limit of applicability of the treatment by Zhang and Duan (2005) may be about 60 kb, based on a comparison of molecular dynamics and AIMD calculations (Pan et al., 2013). At greater pressures, the treatment by Zhang and Duan (2009) appears to be more accurate, but is not appropriate for the lower pressures shown in Fig. 2A. Overall, the equation of state from Zhang and Duan (2005) appears to be the most accurate and useful equation of state for water for $1.0 \leqslant P \leqslant 60.0$ kb. Calculated values are listed in Appendix 1.

2.2. Application of the Franck et al. (1990) equation to predicting values of (ε_{H_2O}) for $\rho_{H_2O} < 1.1$ g cm^{-3}

Franck et al. (1990) demonstrated that an equation derived from statistical mechanics for the dielectric constant of a hard-sphere fluid was applicable to water and other fluids at densities up to 1.1 g cm^{-3}. Below 400 °C and at densities higher than 1.1 g cm^{-3} the Franck et al. equation is

inadequate (Dolejš, 2013). The equation expressed (ε_{H_2O}) in terms of T (K) and ρ_{H_2O} (g cm^{-3}) with only two molecular parameters needed, the dipole moment (μ_{H_2O}) and the diameter of the water molcule (σ_{H_2O}):

$$\varepsilon - 1 = \frac{3y}{1 - a_1 y}[1 + (1 - a_1)y + a_2 y^2 + a_3 y^3] \quad (1)$$

where

$$a_1 = 0.4341\rho^{*2} \quad (2)$$

$$a_2 = -(0.05 + 0.75\rho^{*3}) \quad (3)$$

$$a_3 = -0.026\rho^{*2} + 0.173\rho^{*4} \quad (4)$$

$$y = (4\pi/9)\mu^{*2}\rho^{*} \quad (5)$$

where

$$\mu^{*2} = \mu^2_{H_2O}/kT\sigma^3_{H_2O} \quad (6)$$

and

$$\rho^{*} = \rho\sigma^3_{H_2O}N_A \quad (7)$$

The calibration of Eq. (1) was carried out in the present study using experimental data for and estimates of (ε_{H_2O}) at the highest temperatures possible so that the upper limit of the density of 1.1 g cm^{-3} would correspond to the highest pressures. The range of pressures and temperatures used can be seen in Fig. 3. The highest temperature experimental data are at 550 °C (Heger et al., 1980). These data were simultaneously regressed with estimates from a comprehensive assessment and fitting procedure which extended to 927 °C (Fernández et al., 1997). The intermediate temperature of 727 °C was included because recent AIMD calculations were carried out at that temperature (Pan et al., 2013).

In the original implementation of Eqs. (1)–(7), Franck et al. (1990) obtained values for μ_{H_2O} and σ_{H_2O} of 2.33 D and 2.68 Å, respectively, based on fitting data from Heger et al. (1980) and a thesis by Deul (see Franck et al., 1990) at 400 and 500 °C. Our calibration of Eq. (1) using the much larger temperature range in Fig. 3 resulted in values of 2.39 D and 2.34 Å, respectively, very similar to those of Franck et al. (1990). The use of a constant dipole moment, in accordance with the SPCE (Extended Simple Point Charge) water model, is reasonable given the limited pressure and temperature ranges for the application of Eq. (1). It can be seen in Fig. 3 that the theoretically calculated curves agree with the data points within about 10%. For example, at 550 °C the maximum discrepancy with the experimental data of Heger et al. (1980) corresponds to about 400 cal mol^{-1} in the HKF equation for the standard Gibbs free energy of an aqueous species with a typical Born solvation coefficient ω (Appendix 1) of 1.0×10^5 cal mol^{-1}. This would result in a discrepancy of about 0.1 log K units for a reaction involving this aqueous species, which is comparable to small experimental uncertainties in solubility and speciation measurements.

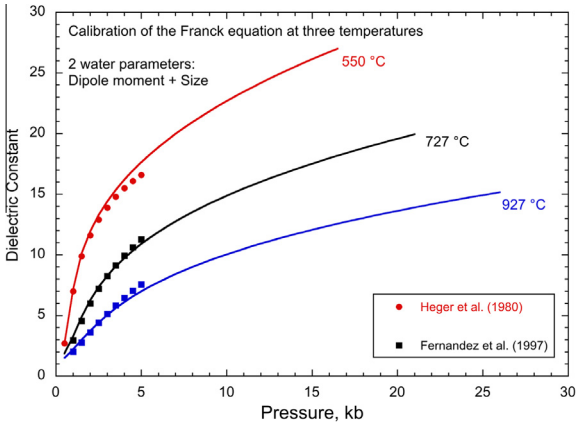

Fig. 3. Calibration of the Franck et al. (1990) equation for (ε_{H_2O}) using experimental data from Heger et al. (1980) and values from a synthesis by Fernandez et al. (1997). The curves represent calculated values of (ε_{H_2O}) using the calibrated Franck et al. equation up to a density of 1.1 g cm^{-3} at each temperature.

2.3. Extrapolation of dielectric constants to 60 kb

Although the application of Eqs. (1)–(7) greatly expands the range of pressures over which the HKF equations could be used, the upper limit of 1.1 g cm^{-3} for Eq. (1) still imposes pressure limits at elevated temperatures that prevent application to a broad range of upper mantle conditions (e.g. Fig. 3). Previous studies of the dielectric constant of water have emphasized that the available experimental data closely follow linear correlations between $\ln(\varepsilon_{H_2O})$ versus $\ln\rho_{H_2O}$ up to 5 kb or more (e.g. Helgeson and Kirkham, 1974a; Marshall, 2008; Dolejš, 2013). The validity of such empirical correlations can now be tested for much higher pressures by using the results of recent AIMD calculations.

The points plotted in Fig. 4 represent results from Pan et al. (2013). The values of $\ln(\varepsilon_{H_2O})$ from the calculations are plotted versus values of $\ln\rho_{H_2O}$ which are an exact feature of the calculations (i.e. known from the number of molecules in the theoretical box used). Although there are only three points, they show a very strong correlation, suggesting that the assumption of linearity holds to very high pressures. This result in turn supports the use of such linear correlations to extrapolate values of (ε_{H_2O}).

In the present study, we assume that similar empirical linear correlations hold over a wide range of pressures and temperatures and can be used to extrapolate values

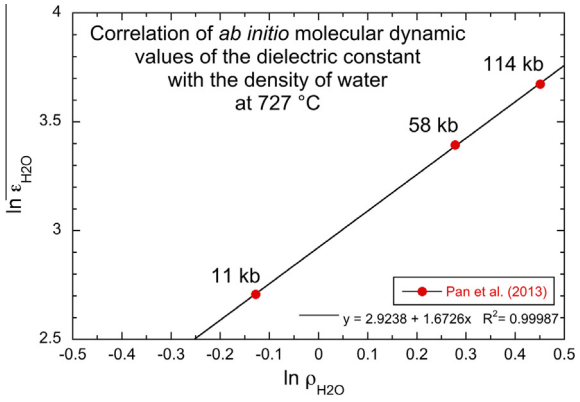

Fig. 4. Empirical correlation of AIMD results for (ε_{H_2O}) at 727 °C (Pan et al., 2013) with the corresponding densities in the simulations. The line represents a regression using the three points.

of $\ln(\varepsilon_{H_2O})$ calculated with the Franck equation to densities much greater than 1.1 g cm^{-3}. It can be seen in Fig. 5A that values of $\ln(\varepsilon_{H_2O})$ are plotted from experimental studies referring to temperatures from 25 to 550 °C (Cogan, 1958; Heger et al., 1980; Deul, 1984) and show a strong linear correlation with $\ln\rho_{H_2O}$. At the higher temperatures of 600 to 1000 °C, values of $\ln(\varepsilon_{H_2O})$ calculated with the Franck equation (Eqs. (1)–(7)) using our values for μ_{H_2O} and σ_{H_2O} of 2.39 D and 2.34 Å also show a strong correlation of $\ln(\varepsilon_{H_2O})$ versus $\ln\rho_{H_2O}$ up to $\rho_{H_2O} = 1.1$ g cm^{-3}. Values of ρ_{H_2O} were calculated as discussed above with equations in Zhang and Duan (2005).

It should be emphasized that the data points in Fig. 5A at temperatures greater than 600 °C are based on the calibration of the Franck et al. equation with estimates made using the Fernández et al. equations. For temperatures less than 200 °C in Fig. 5A, the limited amount of data depicted are not meant to represent a comprehensive survey of the data available, as the main focus of this paper is elevated temperatures and pressures. Instead, they are included to ensure that the completely empirical equation of state for (ε_{H_2O}) being developed here has a sensible behavior approaching 25 °C. We also emphasize that we used the experimental data from Heger et al. (1980) as much as possible because that will give closer agreement with the values of (ε_{H_2O}) calculated in the code SUPCRT92 (Johnson et al., 1992). However, as previously noted in the comprehensive study by Fernández et al. (1997), it appears that not all the Heger et al. data are consistent with the rest of the data from the literature. Similarly, in our more empirical treatment, we found that the highest pressure data from Heger et al. (1980) at 5.0 kb were not consistent with the Franck equation and were omitted from Fig. 5A. This ultimately resulted in small discrepancies with the Heger et al. data at 5 kb (see Fig. 6B below). None of these discrepancies can be resolved until new experimental measurements of (ε_{H_2O}) become available. Until then, the empirical correlations given in Fig. 5 serve as a first approximation to (ε_{H_2O}) over a wider range of temperatures and pressures than previously calculated.

The slopes and the intercepts of the lines in Fig. 5A are plotted versus temperature in Fig. 5B and C, respectively.

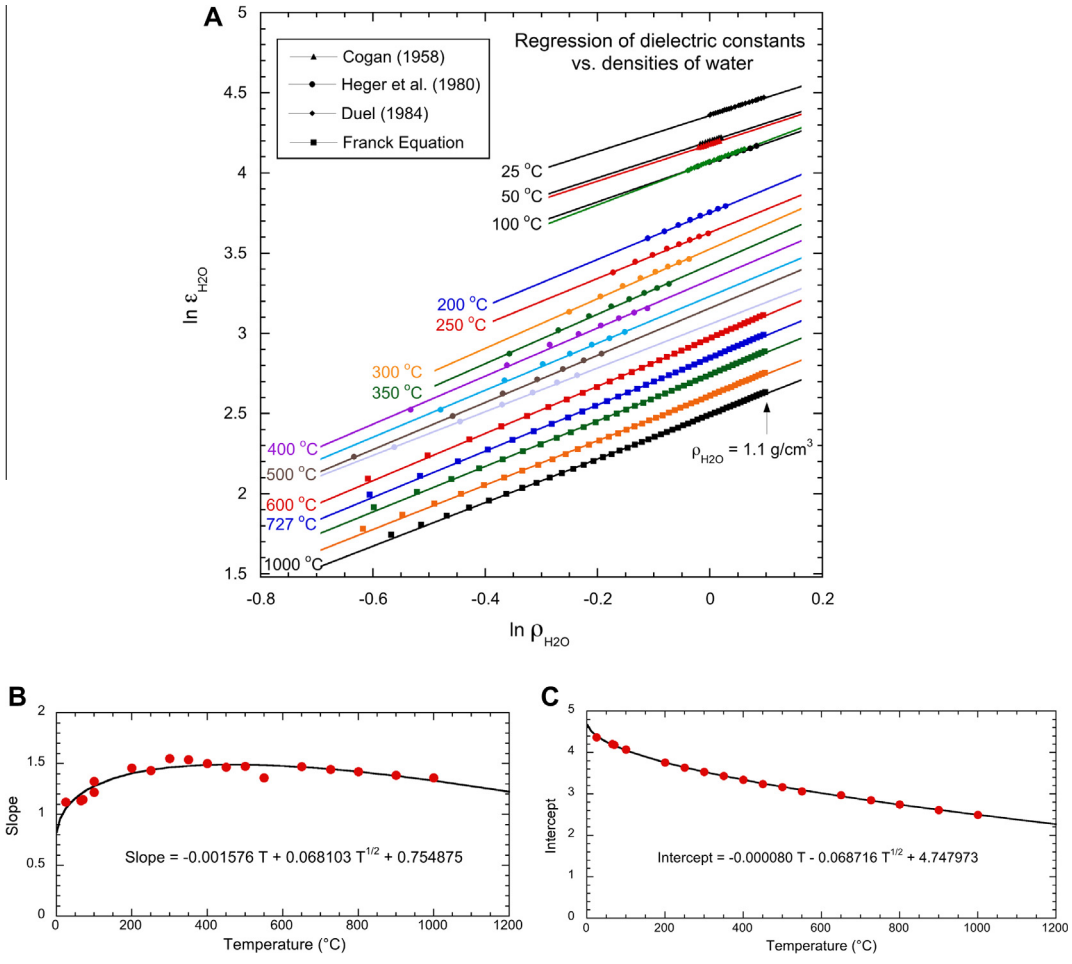

Fig. 5. Regression of values of $\ln(\varepsilon_{H_2O})$ versus $\ln\rho_{H_2O}$ over a wide range of temperatures and pressures: (A) Experimental values of (ε_{H_2O}) were used at temperatures from 300 to 550 °C (Heger et al., 1980); values calculated with the Franck et al. (1990) equation were used at temperatures from 600 to 1000 °C. (B) Slopes of the regression lines in (A) versus the temperature. (C) Intercepts of the lines in (A) versus temperature.

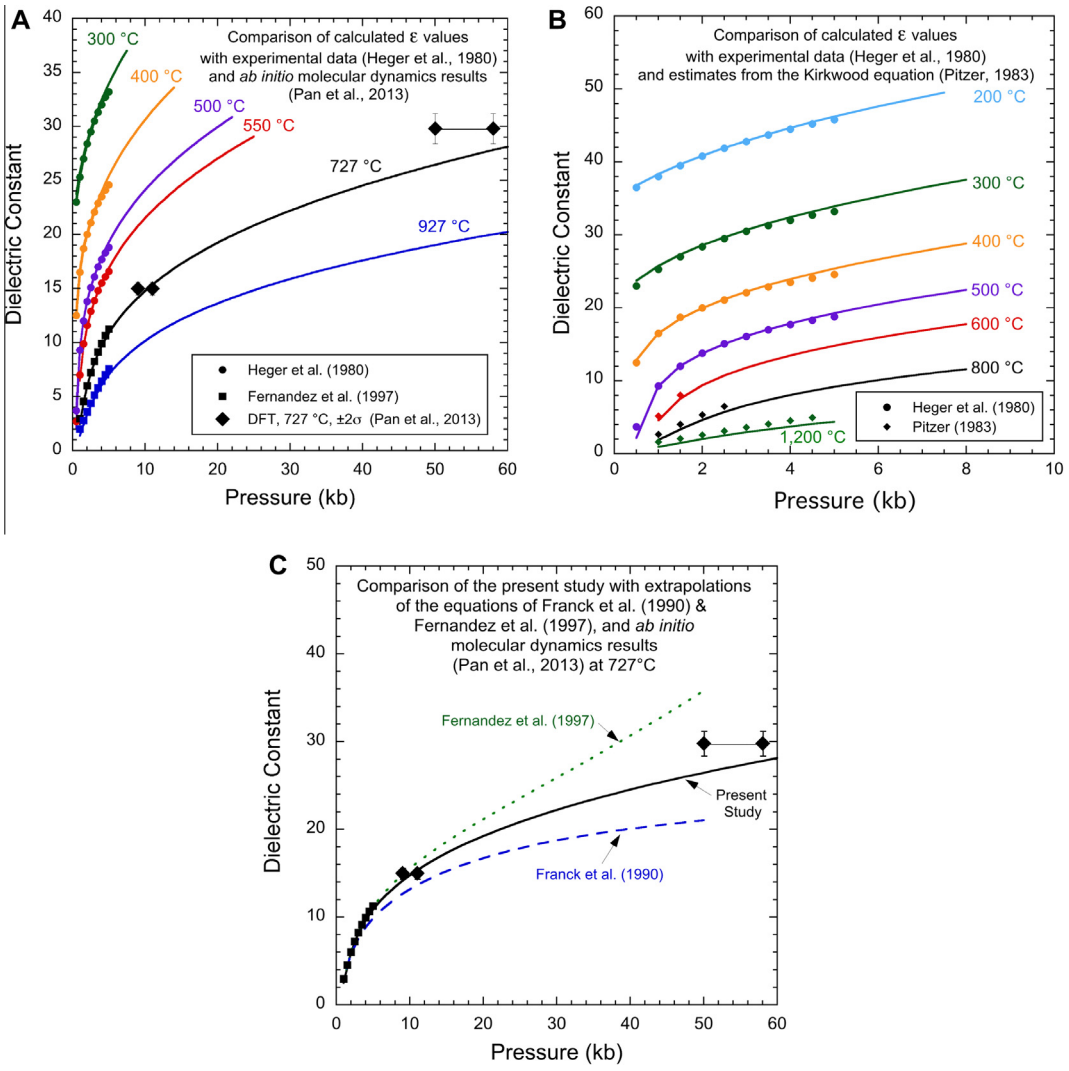

Fig. 6. Comparison of the new empirical equation for the dielectric constant, based on empirical extrapolation of the Franck et al. (1990) equation for (ε_{H_2O}) with AIMD results at 9–10 and 50–58 kb, experimental data from Heger et al. (1980) at 300 to 550 °C, and estimates from the synthesis of Fernandez et al. (1997) at 727 and 927 °C and Pitzer (1983) at 600, 800 and 1200 °C.

The smooth distribution of the points on these graphs provides support for the application of a power function fit that can be used to generate values of (ε_{H_2O}) over wide ranges of temperature and pressure. The full relation between the dielectric constant and the density of water can be written as:

$$\varepsilon_{H_2O}(\rho, T[^\circ C]) = \exp(b_1 T + b_2 T^{1/2} + b_3)\rho^{(a_1 T + a_2 T^{1/2} + a_3)} \quad (8)$$

where the density is in g cm^{-3} and the temperature (T) is in °C. The parameters a_i and b_i are listed in Table 1. We emphasize that Eq. (8) is completely empirical and should only be used between 100 and 1200 °C when the pressure is at least 1.0 kb. It was selected because of its simplicity and the relatively small number of fit parameters, as well as its ability to extrapolate smoothly to at least 1200 °C at pressures from 1.0 to 60 kb. Extrapolations were not made below 1.0 or above 60 kb in the present study because of the likely inaccuracies of the density of water calculated with the treatment of Zhang and Duan (2005) at such pressures (see above). Calculated values of (ε_{H_2O}) and ρ_{H_2O} are given in Appendix 2.

Table 1
Polynomial coefficients for computing the dielectric constant of water as a function of the density (ρ, g cm^{-3}) and the temperature (T, °C) to be used for temperatures greater than 100 °C when the pressure is greater than 1.0 kb.

Fit parameters for the equation:
$\varepsilon(\rho, T[^\circ C]) = \exp(b_1 T + b_2 T^{1/2} + b_3)\rho^{(a_1 T + a_2 T^{1/2} + a_3)}$

Slope		Intercept	
a_1[a]	-1.576377×10^{-3}	b_1[a]	-8.016651×10^{-5}
a_2[b]	$+6.810288 \times 10^{-2}$	b_2[b]	-6.871618×10^{-2}
a_3	$+7.548755 \times 10^{-1}$	b_3	$+4.747973 \times 10^{+0}$

[a] °C^{-1}.
[b] °C$^{-0.5}$.

2.4. Comparison with *ab initio* molecular dynamics results

Recent *ab initio* molecular dynamics calculations have presented predictions of the dielectric constant at elevated temperatures and pressures as indicated above (Pan et al., 2013). These results offer a test of the high-pressure extrapolations of our new dielectric constant equation of state and comparisons with other suggested estimations. Within the range of applicability for our equation, there are data points at 727 °C and pressures of 11 and 58 kb. These pressures represent the theoretically estimated pressures in the AIMD calculations, which are subject to a significant uncertainty (in contrast to the densities which are known exactly). For this reason, an independent estimate of the pressures at the two densities based on the known temperature and density and the equation of state for water is also plotted in Fig. 6A. Some of the experimental data and estimates used to calibrate the Franck equation (Fig. 2) and the linear correlations (Fig. 5A) are also included as points in Fig. 6A. The solid curves in Fig. 6A represent calculations made using Eq. (8). At 727 °C, it can be seen that the predicted values of (ε_{H_2O}) differ from Pan et al. (2013) by 2.4% at 11 kb and 6.7% at 58 kb. The latter discrepancy would lead to uncertainty in the equilibrium constant of an aqueous species of about 0.06 units at this temperature assuming a Born solvation coefficient ω of 1.0×10^5 cal mol^{-1}.

A more detailed comparison of the calculated values of (ε_{H_2O}) with the experimental data from Heger et al. (1980) and the estimates generated by Pitzer (1983) are shown in Fig. 6B. It can be seen in the figure that discrepancies start to appear at temperatures greater than 500 °C and pressures of less than 1.0 kb. Consequently, it is recommended that Eq. (8) not be used at less than 1.0 kb for temperatures greater than 500 °C. It can also be seen in the figure that the present study produces values of (ε_{H_2O}) at 800 and 1000 °C that are systematically lower than those estimated by the Pitzer approach. Which of the two approaches is more accurate will have to await the availability of experimental data or quantum chemical calculations at these very high temperatures and relatively low densities. Overall, the small discrepancies between the solid curves and the solid points at all temperatures with pressures greater than 1.0 kb emphasize the wide-ranging applicability of the present results.

Finally, a comparison of the dielectric constant calculated in the present study with extrapolations of the Fernández et al. (1997) and Franck et al. (1990) equations is given in Fig. 6C. At 727 °C from 2.0 to over 50 kb, it is clear that the Franck et al. (1990) equation (calibrated as discussed in the present study) results in values too low compared to the *ab initio* molecular dynamics calculations. However, the Fernández et al. equation gives results that are too high compared to the *ab initio* molecular dynamics calculations. A similar result would be obtained with the empirical equation of Marshall (2008), which shows close agreement with extrapolations of the Fernández et al. equation (Dolejš, 2013). Until experimental data become available, the results of the present study appear to give the most reasonable agreement with as much experimental data as possible at low pressures together with the results of the *ab initio* molecular dynamics calculations at very high pressures.

3. APPLICATION OF THE EXTENDED HKF EQUATIONS TO MINERAL SOLUBILITIES AND AQUEOUS SPECIATION AT HIGH PRESSURES

Extensive experimental work over the last twenty years has been carried out to measure the aqueous speciation and solubilities of various minerals at pressures up to about 20 kb and high temperatures. These advances have far outpaced theoretical work with the HKF equations of state which could be used to extract a fundamental thermodynamic characterization of the aqueous species involved at high pressures and temperatures. Consequently, we have applied our new equation for the dielectric constant in the revised HKF equations of state to help analyze the speciation and solubility measurements. Two geogically important sets of data concern the speciation and solubility of Si and Al.

3.1. Solubility of silica and aqueous silica speciation

3.1.1. Raman evidence for silica speciation and measurements of quartz solubility

The solubility and speciation of aqueous silica at elevated temperatures and pressures has long been of interest (Morey et al., 1962; Weill and Fyfe, 1964; Anderson and Burnham, 1965; Crerar and Anderson, 1971; Walther and Helgeson, 1977; Hemley et al., 1980; Walther and Orville, 1983; Shock et al., 1989; Manning, 1994; Rimstidt, 1997; Zotov and Keppler, 2000, 2002; Newton and Manning, 2002a,b, 2003, 2008, 2009; Mysen, 2010; Mysen et al., 2013b; Hunt et al., 2011; Hunt and Manning, 2012; Spiekermann et al., 2012), but until recently definitive evidence of specific species has been lacking. Application of the HKF equations of state to characterizing the properties of aqueous silica species have assumed that quartz solubility experiments could be interpreted in terms of a single silica species – the silica monomer (Walther and Helgeson, 1977; McKenzie and Helgeson, 1984; Shock et al., 1989). This assumption is the basis for the HKF equation of state characterization of aqueous silica in SUPCRT92. However, it is now clear that a dimer and possibly additional higher order polymeric aqueous species of silica can exist in equilibrium with quartz (Newton and Manning, 2000; Zhang and Frantz, 2000; Zotov and Keppler, 2000, 2002; Mysen, 2010; Hunt and Manning, 2012; Spiekermann et al., 2012; Mysen et al., 2013b). Consequently, a goal of the present study was to develop new HKF equation of state characterizations of aqueous silica species consistent with recent experimental data.

Solubility and speciation data for aqueous silica at high pressures differ between Zotov and Keppler (2002), Manning (1994) and Mysen (2010). However, the speciation data of Mysen (2010) have been interpreted using solubility data extrapolated from Manning (1994). Consequently, as a first step in characterizing the HKF coefficients for the aqueous silica monomer and dimer at high pressures, we have used speciation data from Mysen (2010) together with solubility data from Manning (1994). Data from the Raman spectroscopic study of silica speciation by Mysen (2010) were used to constrain HKF equation

of state representations of the aqueous monomer and dimer of silica. The speciation data have been expressed here as α-quartz solubility reactions represented by

$$SiO_2^{Qtz.} + 2H_2O = Si(OH)_4^0 \quad (9)$$

and

$$2SiO_2^{Qtz.} + 3H_2O = Si_2O(OH)_6^0 \quad (10)$$

for the monomer and the dimer, respectively. The data corresponding to Eqs. (9) and (10) are shown in Fig. 7A and B using thermodynamic properties for α-quartz obtained independently (Berman, 1988). Other characterizations (Helgeson et al., 1978; Robie and Hemingway, 1995; Holland and Powell, 2011) of the thermodynamic properties of quartz do not differ significantly over the pressure–temperature range of the experimental data treated here. Two additional important constraints on the calculations to be discussed were used: an experimental measurement of the silica monomer–dimer equilibrium at 25 °C and 1 bar (Sjoberg, 1996), and a measurement of the solubility of α-quartz assuming it was in equilibrium with the silica monomer at 25 °C and 1 bar (Rimstidt, 1997). Combination of these two constraints gave the standard Gibbs free energies of formation of the silica monomer and dimer at 25 °C and 1 bar (Table 2). Activity coefficients for all neutral aqueous species are assumed to be unity in this study.

It should be noted that the formally dehydrated monomer and dimer properties are given in Table 2. These are defined by the reactions.

$$SiO_{2,aq}^0 + 2H_2O = Si(OH)_{4,aq}^0 \quad (11)$$

and

$$Si_2O_{4,aq}^0 + 3H_2O = Si_2O(OH)_{6,aq}^0 \quad (12)$$

Eqs. (11) and (12) merely represent a convention according to which the properties of the hydrated species on the right-hand side of each equation are calculated from the

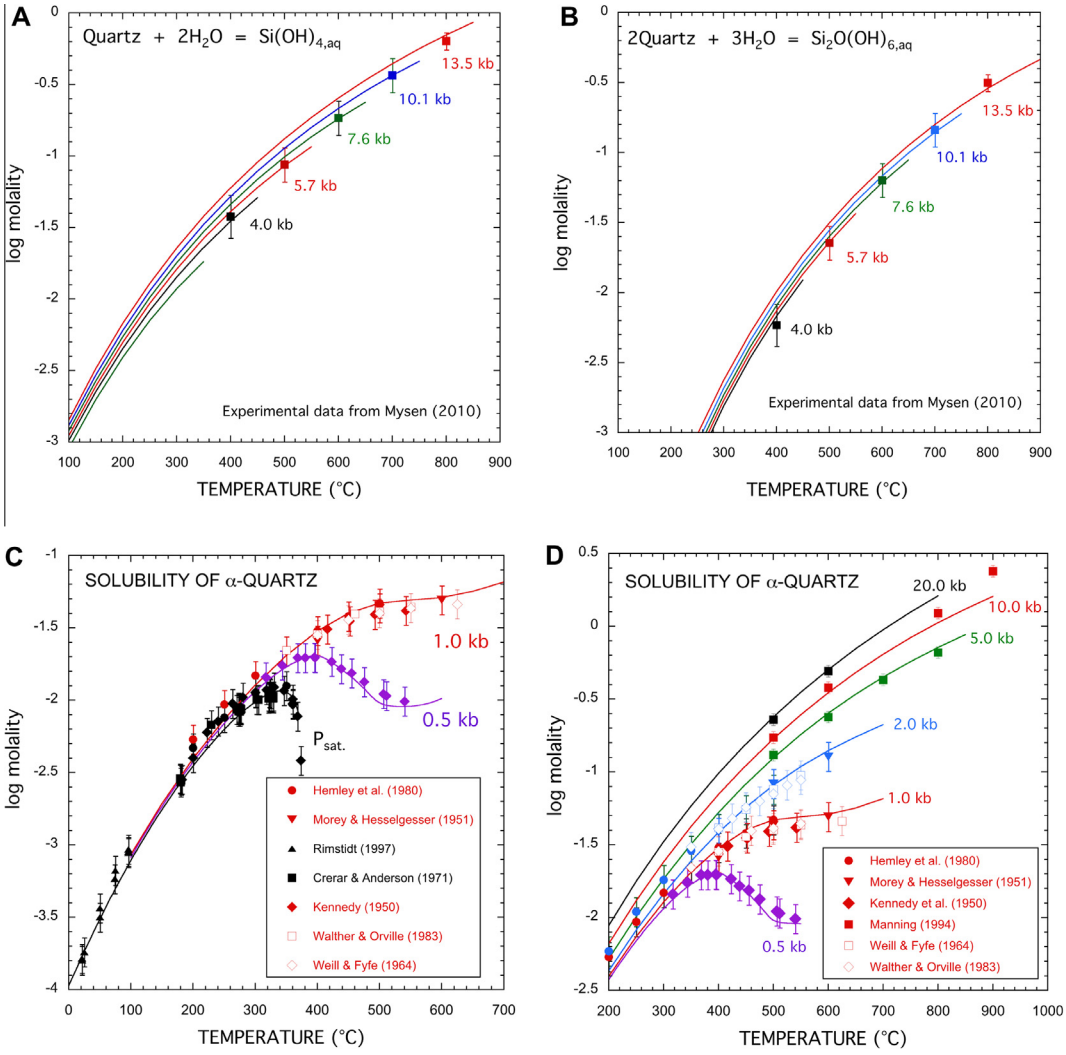

Fig. 7. Experimental data points for the solubility of quartz compared with calculated curves constrained to fit the experimental data. (A) Solubility of quartz as the monomer species. (B) Solubility of quartz as the dimer species. (C) Total solubility of quartz versus temperature at low pressures. (D) Total solubility of quartz versus temperature at high pressures.

Table 2
Equation of state coefficients for use in the revised HKF equations of state for aqueous species consistent with the equilibrium constants given in the Appendices. The parameters are based on regression calculations and correlations (see text).

Species	ΔG_f^0 [a]	ΔH_f^0 [a]	S^0 [b]	C_P^0 [b]	V^0 [c]	$a_1 \times 10$ [d]	$a_2 \times 10^{-2}$ [a,i]	a_3 [e,j]	$a_4 \times 10^{-4}$ [f,k]	c_1 [b,l]	$c_2 \times 10^{-4}$ [f,m]	$\omega \times 10^{-5}$ [a]
$SiO^0_{2,aq}$	−199,560[g]	−213,940	5.3[h]	27.7[h]	18.0[h]	4.9[h]	1.41[i]	4.41	−2.84	25.7	2.6	0.36[h]
$SiO_2O^0_{4,aq}$	−400,760[g]	−427,300	18.0[h]	49.0[h]	40.0[h]	10.1[h]	2.69[i]	0.67	−2.89	35.8	7.0	0.10[h]
$AlO(OH)aq^0$	−207,500[n]	−228,400	−6.5[n]	47.5[o]	13.0[o]	4.3[p]	−0.20	5.01	−2.77	38.6	6.6	0.50[o]
AlO_2^-	−198,700[n]	−222,140	−7.2[n]	−9.5[n]	10.0[n]	4.3[p]	2.50	−1.83	−2.88	19.1	−6.2	1.74[n]
KOH_{aq}	−102,800[q]	−103,530	37.7[q]	21.6[q]	−13.5[q]	5.9[p]	1.34	3.71	−2.83	1.94	−5.8	0.40[q]
$BO(OH)^0_{aq}$	−174,860[r]	−187,400	24.0[s]	3.8[s]	20.5[s]	5.5[s]	1.38	3.10	−2.84	25.0[s]	−10.0[s]	0.10[s]
BO_2^-	−162,240[r]	−184,600[r]	−8.9[t]	−9.0[t]	−16.0[t]	−0.86[t]	−2.60[t]	3.70	−2.67	17.1	−4.9	1.76[t]

[a] cal mole^{-1}.
[b] cal mole^{-1} K^{-1}.
[c] cm^{-3} mole^{-1}.
[d] cal mole^{-1} bar^{-1}.
[e] cal K mole^{-1} bar^{-1}.
[f] cal K mole^{-1}.
[g] Calculated from log$K = -3.74$ for the solubility of quartz as the monomer at 25 °C and 1 bar (Rimstidt, 1997) and log$K = 1.2$ for the aqueous monomer–dimer equilibrium (Sjoberg, 1996).
[h] Regression of Raman speciation and quartz solubility data in Figs. 7A–D and 8A.
[i] Calculated from a_1 and an estimate of σ using Appendix Eqs. (5) and (8), unless otherwise noted.
[j] Calculated from $\overline{V}^0$, a_1, a_2, a_4 and ω using Appendix Eq. (1).
[k] Calculated from a_2 using Appendix Eq. (9).
[l] Calculated from $\overline{C}^0_P$, c_2 and ω using Appendix Eq. (2).
[m] Calculated from $\overline{C}^0_P$ using Appendix Eq. (10).
[n] Pokrovskii and Helgeson (1995) and Shock and Helgeson (1988).
[o] Regression of corundum solubility data in Fig. 10A and B.
[p] Estimated from the new correlation with $\Delta\overline{V}^0_n$ for complexes and neutral species in Eq. (16).
[q] Regression of experimental dissociation constants from Ho and Palmer (1997).
[r] Shock and Helgeson (1988).
[s] $\overline{S}^0$ was obtained from regression of experimental pK values of Mesmer et al. (1972) using the parameters for BO_2^-, given in the table; $\overline{C}^0_P$ was calculated from c_1, c_2 and ω using Appendix Eq. (2); c_1, c_2 and ω were obtained by regression of experimental heat capacity data (Hnedkovsky et al., 1995); $\overline{V}^0$ calculated using Appendix Eqs. (3), (4), and (7) and values of σ and ξ obtained from regression of experimental values of $\overline{V}^0$ as a function of T (Ellis and McFadden, 1972; Ward and Millero, 1974) and ω; the value of a_1 was calculated using Eq. (16) and a value of $\Delta\overline{V}^0_n$ calculated with Appendix Eq. (4).
[t] $\overline{C}^0_P$was obtained from regression of experimental pK values of Mesmer et al. (1972) using the parameters for $BO(OH)^0_{aq}$ given in the table; $\overline{V}^0$ calculated from the σ and ξ values given by Shock and Helgeson (1988) together with their value of ω; the value of a_1 was calculated using Appendix Eq. (5), σ, and a value of a_2 predicted from a value for $\Delta\bar{\kappa}^0_{n,BO_2} = -39.6 \times 10^{-4}$ cm^3 mole^{-1} bar^{-1}, which in turn was calculated from the experimental value for the standard partial molal compressibility $\bar{\kappa}^0_{B(OH)_4^-}$ given by Shock and Helgeson (1988).

sums of the properties of the species on the left-hand side in each case. The dehydrated species $SiO^0_{2,aq}$ and $Si_2O^0_{4,aq}$ are used because the standard partial molal properties of these species correlate with equation of state coefficients developed by Shock and Helgeson (1988) and Sverjensky et al. (1997). Such correlations are the basis of prediction in the absence of experimental standard partial molal volumes and heat capacities and have been used for most of the aqueous species in the data file for SUPCRT92.

The solid curves shown in Fig. 7A–D were generated by simultaneous regression of the Raman speciation data in Fig. 7A and B and the experimentally measured solubilities of α-quartz represented by the symbols in Fig. 7C and D. It should be noted that the solid curves in Fig. 7A and B are anchored at 25 °C and 1 bar by the constraints mentioned above. The regression calculations were used to obtain the standard partial molal properties $\overline{S}^0, \overline{C}^0_P$ and $\overline{V}^0$ and the equation of state coefficients a_1 and ω for the dehydrated monomer and dimer species (Table 2). The values of $\overline{V}^0$ for each species were simultaneously linked to the equation of state coefficients a_2, a_3, a_4, and the values of $\overline{C}^0_P$ were linked to c_1 and c_2 using correlations developed for many aqueous ions and neutral species in Shock and Helgeson (1988, 1990) and Shock et al. (1989) as summarized in Appendix 1.

The regression procedure was possible because of the enormous range of temperatures and pressures covered by the data represented in Fig. 7A–D. Certain of the fitting parameters are more important in some regions of T–P space than others. For example, $\overline{S}^0$ is most reliably obtained from data between 25 and 200 °C. Values of $\overline{C}^0_P$ are most reliably obtained from data between 200 and 900 °C at Psat and pressures greater than about 2 kb. Values of ω are most reliably obtained from data influenced by extreme behavior in the T–P range surrounding the critical point, e.g. between 300 and 360 °C at P_{sat}. and between 350 and 700 °C at pressures from 0.5 kb to 1 kb. Values of $\overline{V}^0$ and a_1 are most reliably obtained from data at greater than 300 °C and pressures from 2 to 20 kb.

Estimated uncertainties in the above parameters retrieved from the high temperature and pressure speciation and solubility data are as follows: $\overline{S}^0$ (± 0.5 cal mol^{-1} K^{-1}), $\overline{C}^0_P$ (± 2 cal mol^{-1} K^{-1}), $\overline{V}^0$ (± 1.0 cm^{-3} mol^{-1}), a_1 (± 0.1 cal mol^{-1} bar^{-1}), and $\omega \times 10^{-5}$ (± 0.05 cal mol^{-1}). Together with previous estimates of the uncertainties in the calculation of standard Gibbs free energies at elevated temperatures and pressures using the HKF equations of state (Shock and Helgeson, 1988), our results are overall consistent with uncertainties of ± 0.3 – ± 0.5 in equilibrium constants for aqueous species at high temperatures and pressures.

It is noteworthy that the value of $\omega_{SiO_{2,aq}}(\times 10^{-5}) = 0.36$/cal mol^{-1} given in Table 2 is well within the overall uncertainties of an experimentally derived value of 0.44 cal mol^{-1} (Dandurand and Schott, 1987). Previously 0.13 was obtained in HKF treatments of aqueous silica (Walther and Helgeson, 1977; Shock et al., 1989) which is outside the uncertainty estimated for our value. Furthermore, the values of a_1 for the monomer and dimer obtained in the present study compare very favorably within uncertainty with the correlation between a_1 and ΔV^0_n at 25 °C and 1 bar for neutral aqueous organic species and aqueous complexes described below. The value of a_1 for the dimer obtained in the present study is not consistent with the original correlation proposed by Shock and Helgeson (1988), as can be seen in comparing the original and revised correlations discussed below.

It can be seen in Fig. 7A–D that close agreement exists between the regression curves and the bulk of the Raman speciation and solubility data. A more extensive comparison with high pressure solubilities is shown in Fig. 8A. Despite the overall close agreement between the calculations and the data, however, systematic discrepancies are apparent at the highest temperatures. It can be seen in Fig. 8A that at $T = 900$ °C and $P \geqslant 7$ kb the calculated curve is systematically lower than the data. This is to be expected because of the likely existence of higher order polymers of aqueous silica independently inferred by a number of studies (Zotov and Keppler, 2000, 2002; Hunt et al., 2011; Hunt and Manning, 2012). Apparently the solubility of quartz under these conditions is so high that the formation of additional polymerized species is enhanced. Consequently, the present equations should be expected to give minimum estimates for the solubilities of silica in mineral–fluid assemblages in equilibrium with quartz at $T > 800$ °C.

A test of the above equation of state characterizations of the aqueous silica monomer and dimer is provided by predicting the solubility of Si in equilibrium with the mafic assemblage enstatite + forsterite. It can be seen in Fig. 8B that close agreement exists between the experimental data (Hemley et al., 1977; Newton and Manning, 2002b) and the predicted curves. It is interesting to note that even at 900 °C the curve in Fig. 8B is slightly lower than the experimental solubilities. This result is consistent with the systematic underestimation in the corresponding quartz system. However, in the enstatite + forsterite + H_2O system, the solubility of Si is much lower than in the quartz + H_2O system. Consequently, it is less favorable for the formation of silica polymers of higher order than the dimer. As a result, the present equations for the monomer and the dimer can be used at temperatures up to at least 900 °C for calculations relevant to mantle assemblages free of a pure silica phase, such as the enstatite + forsterite + H_2O system.

3.1.2. Prediction of aqueous silica speciation to 60 kb and 800 °C

An example of the advantage of developing the HKF equations of state for the aqueous silica species is that they can now be used to make predictions over wide regions of T–P space. Aqueous silica speciation in equilibrium with α-quartz is shown in Fig. 9A and B. It should be noted that the percentage of the total dissolved Si is shown, not the molalities of the monomer and the dimer. In this way, the curves take into account the fact two moles of silica are present per mole of the dimer. In addition, at the higher pressures shown in Fig. 9B, α-quartz is not the stable polymorph of silica. Consequently the curves in Fig. 9B at the highest pressures represent metastable extensions of the sol-

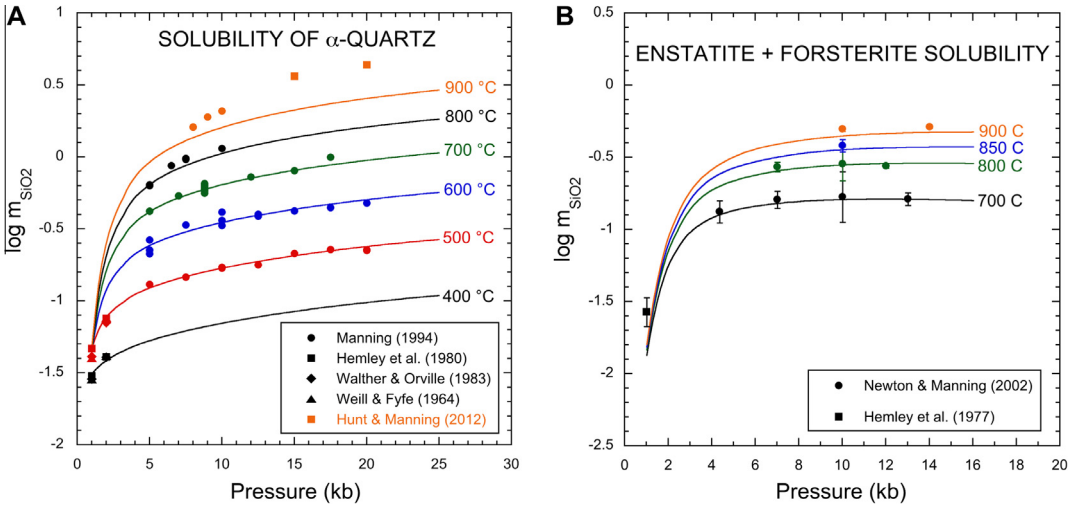

Fig. 8. Experimental data points for the solubility of silica compared with predicted curves. (A) Total solubility of quartz as a function of pressure. (B) Total solubility of enstatite + forsterite as a function of pressure.

ubility of quartz which will be greater than those for the stable polymorph coesite.

It can clearly be seen in Fig. 9A that most of the silica in solution is present as a monomer at temperatures less than about 500 °C. Higher temperatures are predicted to strongly favor the dimer, which is consistent with the Raman speciation data (Fig. 7A and B) and the trend towards increased polymerization with temperature for many different types of molecules (Shock, 1992, 1993). Changes with pressure are illustrated in Fig. 9B where it can be seen that these are much less dramatic than the changes with temperature. The relative proportions of monomer and dimer are not very sensitive to pressure. Again, this is consistent with the very small pressure dependences shown in the Raman data (Fig. 7A and B).

Similar trends are apparent in the silica speciation in equilibrium with enstatite + forsterite in Fig. 9C and D. The major difference between these results and those for the quartz is that the monomer is predicted to be much more important than the dimer over larger regions of *T–P* space for the enstatite + forsterite + H_2O system. This is particularly apparent in comparing Fig. 9B and D. In the latter figure, it can be seen that the silica in solution is predominantly present as monomer at all pressures greater than about 10 kb in the enstatite + forsterite + H_2O system.

3.2. Solubility of corundum and aqueous aluminum speciation

3.2.1. Aqueous Al speciation and solubility studies at low pressures

In contrast to aqueous silica, there are many studies of the speciation of aqueous Al at P_{sat} conditions (Palmer and Wesolowski, 1992; Wesolowski, 1992; Pokrovskii and Helgeson, 1995; Diakonov et al., 1996; Shock et al., 1997; Tagirov and Schott, 2001). Furthermore, unlike the situation for aqueous silica, there are measurements of the standard partial molal heat capacities and volumes of the Al^{3+} and $Al(OH)_4^-$ species as functions of temperature (Hovey and Tremaine, 1986) which are fundamental to the calibrations of the HKF equations of state for these species (Shock and Helgeson, 1988). The two most comprehensive treatments of the thermodynamic properties of the aqueous Al-species as functions of temperature and pressure are those of Pokrovskii and Helgeson (1995) and Tagirov and Schott (2001). In the present study, we build on the work of Pokrovskii and Helgeson (1995) because the HKF equation of state representations of aqueous Al-species were developed using the dehydrated versions of the aqueous Al hydroxide complexes $AlO(OH)^0_{aq}$ and AlO_2^- (see below), which are more appropriate for the estimation of the HKF equation of state coefficients (Shock et al., 1989).

3.2.2. Comparison with experimental solubilities at high pressures

Previous analysis of aqueous Al speciation has indicated that at elevated temperatures, in systems without added silica, the aqueous $Al(OH)^0_{3,aq}$ and $Al(OH)_4^-$ species can be expected to predominate, depending on the pH (Pokrovskii and Helgeson, 1995). These species were also inferred in a series of studies of the solubility of corundum at elevated pressures and temperatures (Tropper and Manning, 2007; Wohlers and Manning, 2009).

As in the case of aqueous silica discussed above, in the present study the dehydrated versions of the aqueous Al hydroxide complexes were used. These are denoted by $AlO(OH)^0_{aq}$ and AlO_2^- and are related to the hydrated conventional hydroxide complexes by the equations

$$AlO(OH)^0_{aq} + H_2O = Al(OH)^0_{3,aq} \quad (13)$$

and

$$AlO_2^- + 2H_2O = Al(OH)_4^- \quad (14)$$

The standard partial molal properties and the equation of state parameters for $AlO(OH)^0_{aq}$ and AlO_2^- given in Table 2 were derived as follows.

For the neutral species $AlO(OH)^0_{aq}$ the values of $\Delta\overline{G}^0_f$, $\Delta\overline{H}^0_f$ and $\overline{S}^0$ were taken from Pokrovskii and Helgeson

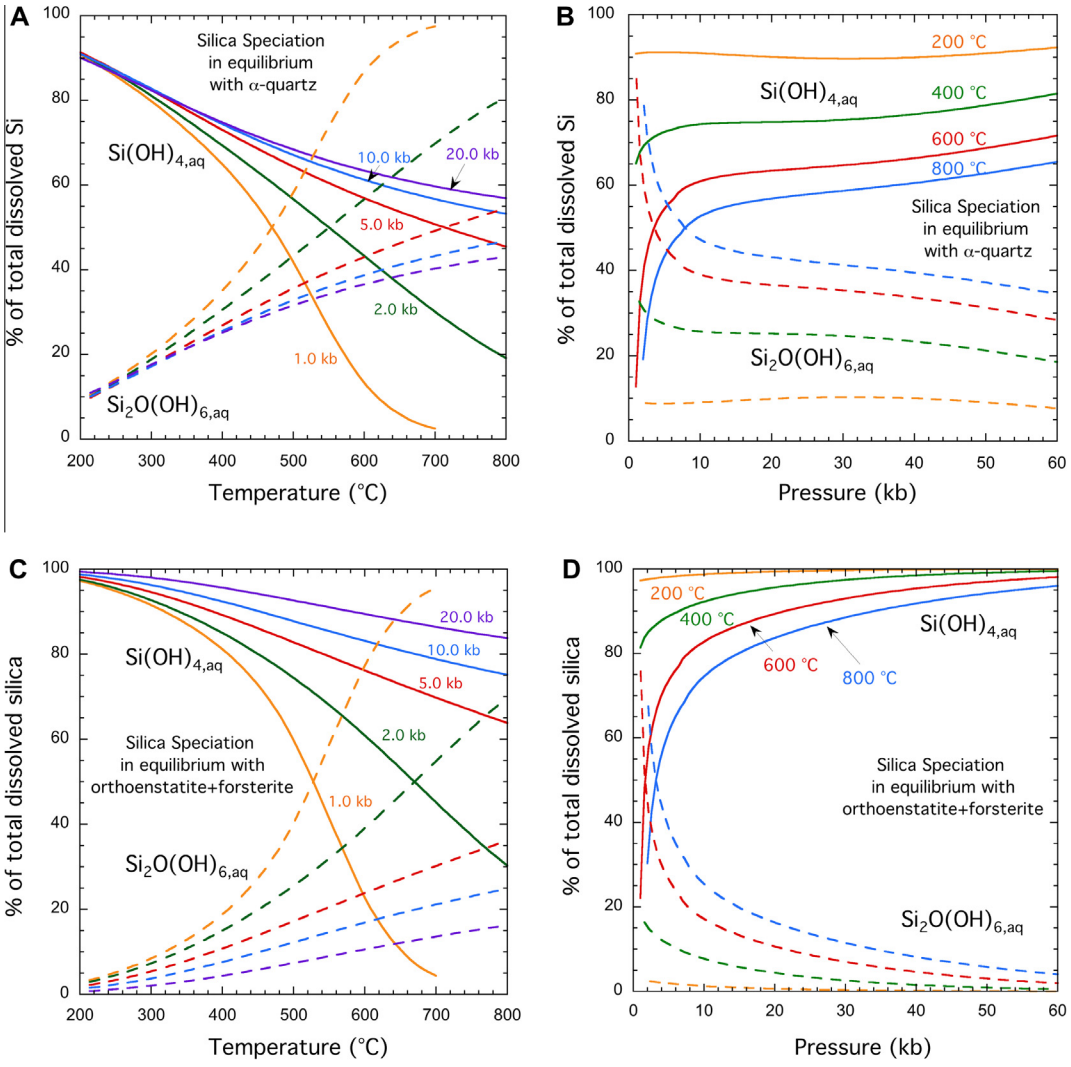

Fig. 9. Predicted speciation of aqueous silica in equilibrium with quartz or enstatite + forsterite as functions of temperature and pressure.

(1995) and combined with estimates of $\overline{C}^0_P, \overline{V}^0$ and ω (Shock et al., 1997) and linear correlations to estimate σ from $\Delta\overline{V}^0_n$, a_4 from a_2, and c_2 from $\overline{C}^0_P$ (Appendix 1, Eqs. (8)–(10)). The value of a_1 was estimated from a new correlation with $\Delta\overline{V}^0_n$ for complexes and neutral species (see Eq. (16) below). The value of a_3 was obtained from $\overline{V}^0, a_1, a_2, a_4$ and ω (Appendix, Eq. (1)). The estimates of $\overline{C}^0_P, \overline{V}^0$ and ω were refined by prediction of the solubility of corundum over a wide range of temperatures and pressures using solubility data (Becker et al., 1983; Tropper and Manning, 2007) which extend over a region of temperatures and pressures where $AlO(OH)^0_{aq}$ is the only important Al species. As in the case of the aqueous silica species discussed above, estimated uncertainties in the above parameters retrieved from the high temperature and pressure speciation and solubility data are as follows: $\overline{S}^0$ (± 0.5 cal mol^{-1} K^{-1}), $\overline{C}^0_P$ (± 2 cal mol^{-1} K^{-1}), $\overline{V}^0$ (± 1.0 cm^{-3} mol^{-1}), a_1 (± 0.1 cal mol^{-1} bar^{-1}) and $\omega \times 10^{-5}$ (± 0.05 cal mol^{-1}).

It can be seen in Fig. 10A and B that the calculated curves show close agreement with the experimental data. The final values for $AlO(OH)^0_{aq}$ of $\overline{C}^0_P$ and ω (47.5 cal mol^{-1} K^{-1} and 0.5 cal mol^{-1}, respectively) differ significantly from those given by Pokrovskii and Helgeson (41.3 cal mol^{-1} K^{-1} and 0.3 cal mol^{-1}, respectively). However, the final value of $\overline{V}^0$ for this species given in Table 2 (13 cm^{-3} mol^{-1} K^{-1}) differs from the value obtained by Pokrovskii and Helgeson (13.3 cm^{-3} mol^{-1} K^{-1}) within uncertainty.

For the charged species AlO^-_2, the values of $\Delta\overline{G}^0_f, \Delta\overline{H}^0_f, \overline{S}^0, \overline{C}^0_P, \overline{V}^0, \sigma, c_1, c_1$ and ω were taken from Pokrovskii and Helgeson (1995) as originally published in Shock and Helgeson (1988). The value of a_1 was estimated from the new correlation with $\Delta\overline{V}^0_n$ for complexes and neutral species (see below). The value of a_3 was obtained from $\overline{V}^0, a_1, a_2, a_4$ and ω (Appendix Eq. (1)). The parameters in Table 2 were used to predict the solubility of corundum in alkaline solutions at 700 °C and 10 kb for comparison with the data reported by Wohlers and Manning (2009). Under conditions of increasingly alkaline solutions, the species AlO^-_2 contributes substantially to the overall solubility.

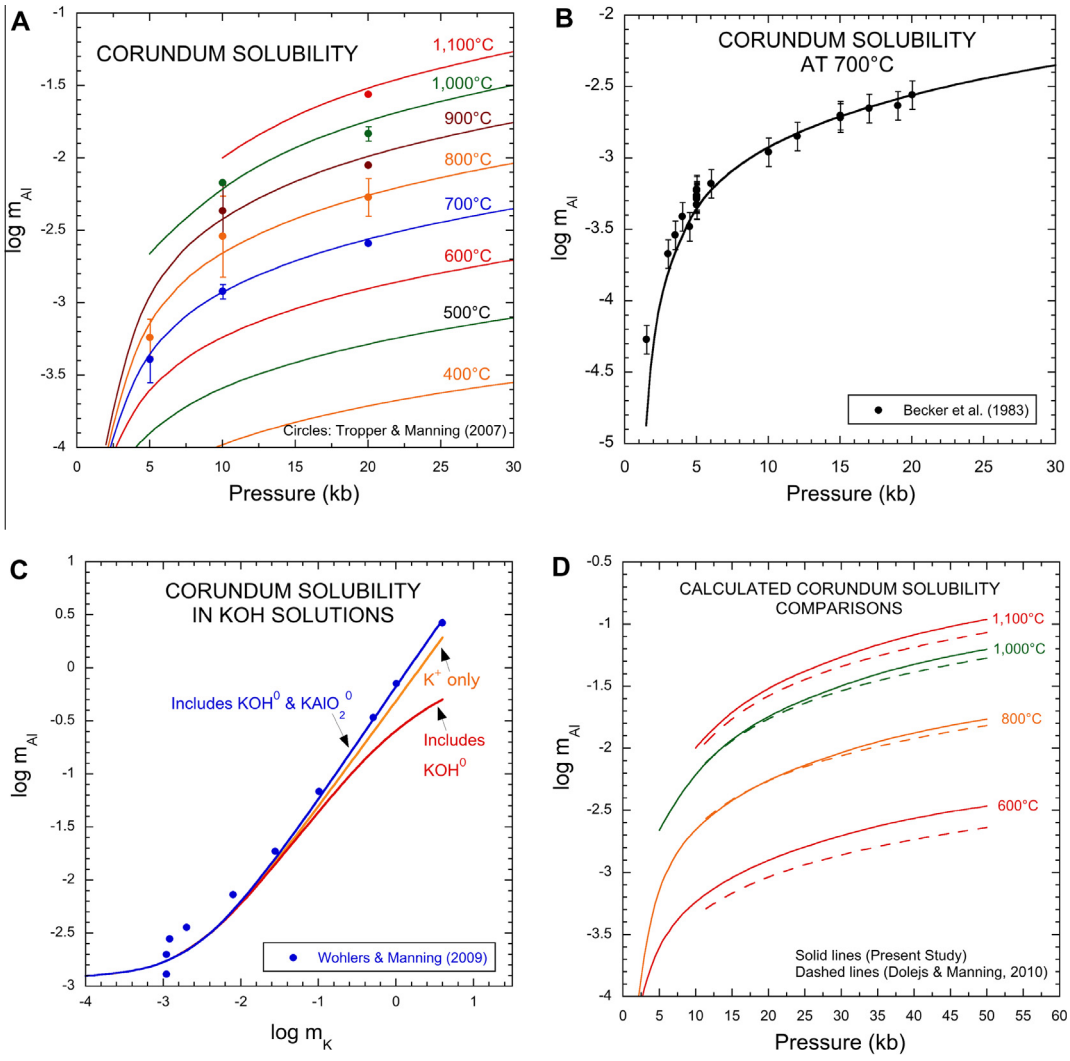

Fig. 10. Experimental and calculated solubilities of corundum. (A) Solubility of corundum in water with temperature and pressure. (B) Solubility of corundum in water as a function of pressure. (C) Solubility of corundum in KOH-solutions: Middle curve (K^+ only) predicted solubility in water without a KOH^0 complex; Lower curve predicted solubility including a KOH^0 complex; Upper curve calculated solubility including KOH^0 and $KAlO_2{}^0$ complexes. (D) Comparison of density model calculations (Dolejš and Manning, 2010) with the present study.

Consequently, the experimental data shown in Fig. 10C provide a good test of the reliability of the equation of state characterization of this species.

As discussed in Wohlers and Manning (2009), the speciation of Al in KOH solutions can be complex at high K concentrations. Accordingly, three calculated curves are depicted in Fig. 10C, corresponding to different aqueous speciation models for the dissolved K. It can be seen in Fig. 10C that the calculated curve for which K^+ is the only K-bearing aqueous species in the model shows quite close agreement with the experimental data from Wohlers and Manning (2009), even without taking into account additional possible complexing in the aqueous phase. A second curve is shown for which the speciation model includes the complex KOH^0_{aq}. The properties of this complex were based on an equation of state fit to published dissociation constant data (Ho and Palmer, 1997) and are summarized in Table 2. It can be seen in Fig. 10C that this curve lies significantly below the experimental solubility data. This is a consequence of lower pH values in the speciation model when the KOH^0_{aq} complex becomes significant relative to K^+. At the lower pH values, the AlO_2^- species becomes less important resulting in lower calculated solubilities. Under these conditions it can be inferred that a $KAlO^0_{2,aq}$ species might be important. The third curve shown in the figure fits the experimental data well over a very wide range of K concentrations. It corresponds to a speciation model that includes KOH^0_{aq} and $KAlO^0_{2,aq}$ with a $\log K = 2.18$ at 700 °C and 10 kb corresponding to the reaction.

$$K^+ + AlO^-_{2,aq} = KAlO^0_{2,aq} \quad (15)$$

Overall, the close fit of the calculated curves in Fig. 10A–C, and the lower temperature and pressure data already fitted by Pokrovskii and Helgeson (1995), provides strong support to the equation of state characterization of the dissolved Al species $AlO(OH)^0_{aq}$ and AlO_2^-.

Fig. 10D provides a comparison of the corundum solubility in water calculated with the density model of Dolejš and Manning (2010) with the solubility calculated in the present study. Both curves have been extrapolated outside the range of temperatures and pressures used to fit the experimental data of Tropper and Manning (2007). Although both curves have a very similar predicted pressure dependence, it can be seen that the temperature dependence is significantly different at 600 and at 1100 °C.

3.2.3. Prediction of aqueous aluminum speciation to 50 kb and 1000 °C

The standard partial molal properties and equation of state coefficients developed above for $AlO(OH)^0_{aq}$ and AlO_2^- now enable prediction of the relative importance of these species over wide ranges of pressure and temperature in equilibrium with any Al-bearing mineral or mineral assemblage. However, recent experimental solubility studies of mixed Na–Al–Si assemblages strongly suggest that $AlO(OH)^0_{aq}$ and AlO_2^- are not the only dissolved Al species (Tagirov and Schott, 2001; Tagirov et al., 2004; Manning et al., 2010; Wohlers et al., 2011). More complex species are indicated by the experimental studies, and may exist in deep fluids in the Earth. The results of the present study should provide a useful platform for analyzing the results of these more complex systems.

In the meantime, it is useful to be able to display the speciation expected for $AlO(OH)^0_{aq}$ and AlO_2^- in equilibrium with corundum over ranges of pressure and temperature not yet studied by experiment. Some examples are shown in Fig. 11A and B. It can be clearly seen in Fig. 11A that at lower crustal temperatures and pressures both $AlO(OH)^0_{aq}$ and AlO_2^- are important. However, in Fig. 11B it can be seen that at very high temperatures and/or high pressures the neutral species $AlO(OH)^0_{aq}$ is predicted to dominate in equilibrium with corundum. In fluids with pH values buffered by aluminosilicate assemblages, that may have lower pH values, these trends could be expected to be amplified. However, the role of more complex species involving Al and Si remains to be investigated in more detail for systems relevant to deep fluids in the Earth.

4. REVISED PREDICTIVE CORRELATIONS FOR HKF EQUATION OF STATE COEFFICIENTS FOR APPLICATION TO HIGH PRESSURES

A special feature of the HKF equations of state for aqueous species is that in the absence of experimental heat capacities and volumes as functions of temperature or pressure it is possible to estimate the equation of state coefficients a_1, a_2, a_3, a_4, c_1, c_2 and ω from correlations with standard partial molal properties referring to 25 °C and 1 bar (Shock and Helgeson, 1988, 1990; Shock et al., 1989). The estimated coefficients can then be used to predict the temperature and pressure dependences of the standard free energies of many hundreds of aqueous species. In turn, these result in prediction of equilibrium constants as functions of temperature and pressure. Overall, this constitutes a highly useful predictive model for aqueous geochemistry. The coefficients are given in the code SUPCRT92 (Johnson et al., 1992) that has been widely used up to 1000 °C and 5.0 kb. Revisions to the predictive correlations for the equation of state coefficients for neutral aqueous organic species were suggested by Plyasunov and Shock (2001), who analyzed newer heat capacity, volume and compressibility data as functions of temperature and pressure.

During the course of the present study and a related study of carbonate speciation to pressures of 60 kb (Facq et al., 2014), it became apparent that at pressures greater than about 10 kb, the standard free energies calculated with the HKF equations become increasingly sensitive to the pressure equation of state coefficient a_1. This sensitivity arises from the fact that the change in the free energy of an aqueous species with pressure from P_r to P (i.e., $\Delta\overline{G}_{P_r \to P^0}$) is proportional to $a_1(P - P_r)$. Consequently, a_1 must be known or estimated to better than ±0.1 cal mol^{-1}-bar^{-1} at elevated pressures and temperatures.

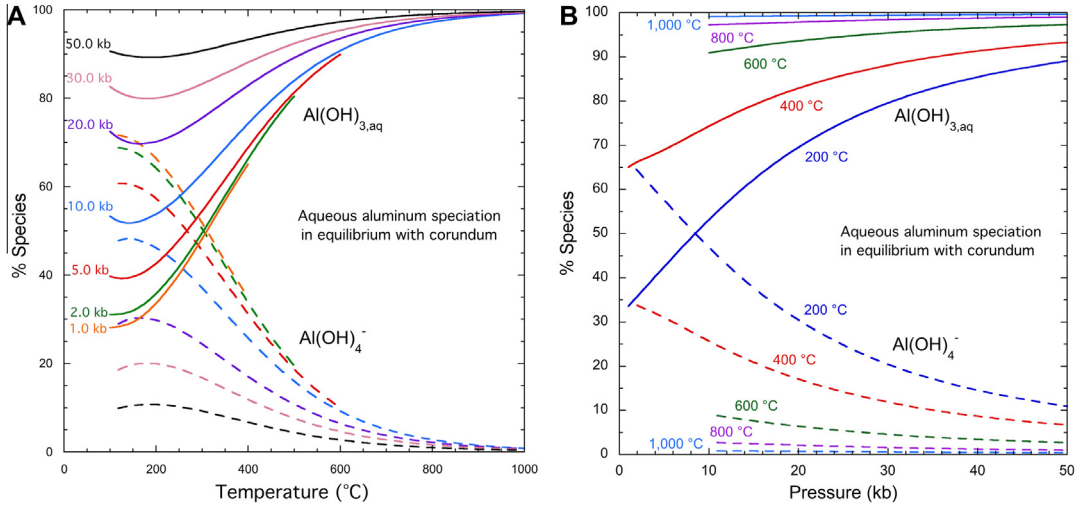

Fig. 11. Predicted speciation of aqueous aluminum in equilibrium with corundum as a function of temperature and pressure.

Values of a_1 have long been estimated from a predictive correlation with ΔV_n^0 at 25 °C and 1 bar (Shock and Helgeson, 1988), based on analysis of experimental values of the temperature dependence of $\Delta\overline{V}_n^0$ and $\Delta\bar{\kappa}_n^0$ for Mg^{2+}, Na^+, K^+, Cl^- and Br^- (Fig. 12A). Although adequate for predictions at pressures of several kb, this correlation can result in highly misleading predictions of the pressure dependence of aqueous protonation, complexing or solubility reactions at pressures of 20–60 kb (Facq et al., 2014). It is now clear that a revision to this correlation should involve a dependence on the charge of the ions (Fig. 12B). Furthermore, theoretical analysis of the a_1 values obtained from experimental values of $\Delta\overline{V}_n^0$ and $\Delta\bar{\kappa}_n^0$ for neutral organic species (Amend and Helgeson, 1997a,b; Plyasunov and Shock, 2001) clearly show that these species also belong on a different correlation to those for simple ions.

In the present study, we build on the results for neutral organic aqueous species of Plyasunov and Shock (2001) by combining the values of a_1 that they report that were based on experimental volume and compressibility data as functions of temperature with results obtained in the present study and from the literature. We included values of a_1 for $SiO_{2,aq}^0$ and $Si_2O_{4,aq}^0$ from our analysis of the extensive solubility and speciation data discussed above, HCO_3^-, HS^- and NH_4^+ (from Shock and Helgeson, 1988, based on σ and the correlation between $\Delta\bar{\kappa}_n^0$ and a_2 at 25 °C and 1 bar), $NaCl^0$ and $MgCl^+$ (based on a re-analysis of data published in Sverjensky et al., 1997), and BO_2^- (based on a re-analysis of the data presented by Shock and Helgeson, 1988, see footnotes to Table 2).

The regression line depicted in Fig. 12C is based solely on the results from Plyasunov and Shock (2001) and is consistent with the equation

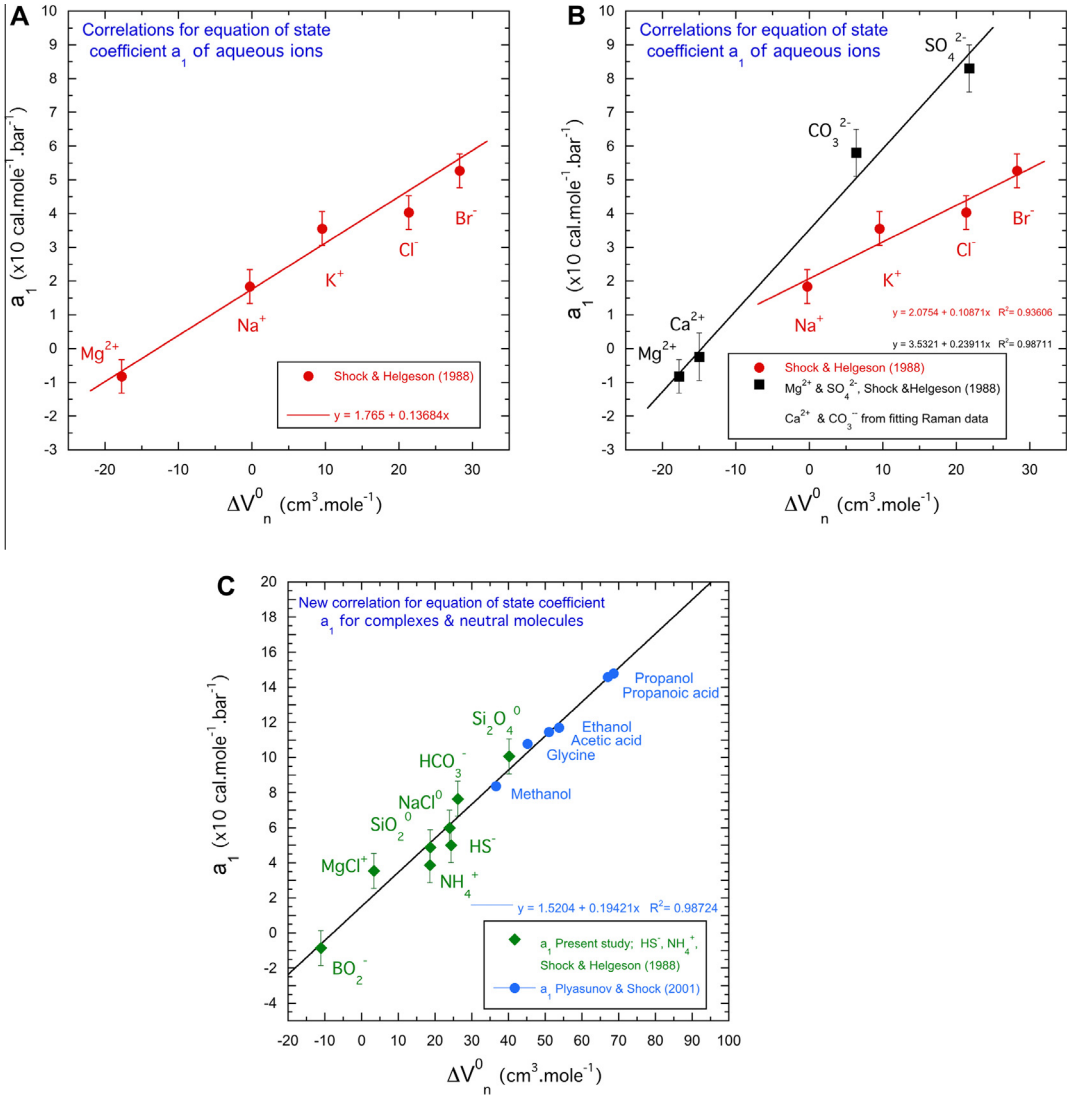

Fig. 12. New correlations for predicting the HKF equation of state coefficient a_1 for aqueous species, which largely governs the pressure dependence of the standard partial molal Gibbs free energy at elevated pressure. (A) Original correlation for aqueous ions from Shock and Helgeson (1988). (B) Revised corelations for aqueous ions (Facq et al., 2014). (C) New correlation established in the present study for neutral species and complexes (Table 2) and published values based on compressibility data for neutral aqueous organic species (Plyasunov and Shock, 2001).

$$a_1(x10) = 0.1942\Delta\overline{V}^0_n + 1.52 \quad (16)$$

where ΔV^0_n is in units of $cm^3\ mol^{-1}$ and a_1 is in units of $cal\ mol^{-1}\ bar^{-1}$. It can be seen in Fig. 12C that the values of a_1 correlate very closely with ΔV^0_n for all complexes and neutral species, both organic and inorganic, typically within the uncertainties represented by the error bars. It should be noted that Eq. (16) was used in defining the values of a_1 for the two aqueous Al-species $AlO(OH)^0_{aq}$ and AlO^-_2 and is clearly consistent with the experimental solubility data for these species for pressures up to 20 kb. Although more high pressure solubility data, as well as data defining the temperature dependencies of both volumes and compressibilities will be necessary to test this correlation, it serves as a useful first step for guiding calculations involving the prediction of aqueous species standard free energies to very high pressures.

5. DEEP EARTH WATER (DEW) MODEL

The combination of the new equation of state for estimating the dielectric constant of water to high pressures, the use of the equation of state for water density from Zhang and Duan (2005), and the revisions to the prediction of the HKF equation of state coefficient a_1 for aqueous species, now enables the predictive calculation of a wide range of equilibrium constants involving many aqueous species to pressures up to 60 kb. These advances have been incorporated into the Deep Earth Water (DEW) model available on the website of the Deep Carbon Observatory as a downloadable spreadsheet.

The DEW model includes a data file for the equation of state coefficients for over 200 aqueous species. Many of these are based on the data file for the code SUPCRT92 as updated in Shock et al. (1997). However, because most of the latter were derived from estimation with predictive correlations originally described in Shock and Helgeson (1988), the equation of state coefficients for species in the DEW model data file were re-estimated using the revised correlations described above.

Included in the DEW model are options to easily change the values of the estimated equation of state coefficients by changing the values of the standard partial molal Gibbs free energy, or the entropy, heat capacity or volume of an aqueous species at 25 °C and 1 bar. This feature of the DEW model enables very fast and flexible modeling of experimental solubility or speciation data: values of the standard partial molal entropy, heat capacity and volume of an aqueous species at 25 °C and 1 bar can quickly be retrieved from experimental data referring to very high temperatures and pressures. In this way, it can be expected that there will be a continuous evolution of our thermodynamic characterizations of aqueous species as functions of temperature and pressure.

6. CONCLUDING REMARKS

A new equation of state for estimating the dielectric constant of water to 60 kb and 1200 °C has been developed by extrapolating values estimated using an equation based on statistical mechanics (Franck et al., 1990) which was calibrated using experimental data from Heger et al. (1980) and estimates from Fernández et al. (1997). The calculated values of (ε_{H_2O}) depend on an equation for the density of water valid from 1 to about 60 kb (Zhang and Duan, 2005). Our predicted values of (ε_{H_2O}) were tested by comparison with the results of *ab initio* calculations (Pan et al., 2013). Expected uncertainties in our predicted values of (ε_{H_2O}) should be minimal for values greater than about 30 at high pressures and may be comparable to most experimental uncertainties in solubility measurements under these conditions.

The predicted values of (ε_{H_2O}) have been used in a comprehensive analysis of aqueous carbonate/bicarbonate speciation in equilibrium with aragonite from 30 to 60 kb (Facq et al., 2014). In the present study, the predicted values of (ε_{H_2O}) were used in the revised HKF equations of state to calculate the standard partial molal Gibbs free energies of the aqueous silica monomer ($SiO^0_{2,aq}$) and dimer ($Si_2O^0_{4,aq}$) and the aqueous Al-species $AlO(OH)^0_{aq}$ and AlO^-_2. The standard free energies were in turn used to analyze a very wide range of experimental speciation and solubility data involving equilibria between quartz + H_2O and corundum + H_2O.

During the course of this analysis, new equation of state parameters were obtained for $SiO^0_{2,aq}$ and $Si_2O^0_{4,aq}$. It is the first time in the long history of the application of HKF-type equation of state treatments to the solubility of quartz and the speciation of Si (Walther and Helgeson, 1977; McKenzie and Helgeson, 1984; Shock et al., 1989) that the equation of state coefficients for aqueous silica species are consistent with correlations with the standard partial molal properties at 25 °C and 1 bar representing a wide variety of experimental data for electrolytes.

Our equation of state characterization of silica species in the presence of quartz is valid to temperatures of about 800 °C at high pressures. At higher temperatures our equations systematically underestimate the solubility of quartz, suggesting the possible existence of higher order polymers of aqueous silica consistent with independent evidence in the literature (Zotov and Keppler, 2000, 2002; Hunt et al., 2011; Hunt and Manning, 2012). However, our equations successfully predict the solubility of silica in equilibrium with enstatite + forsterite + H_2O to 900 °C and 20 kb when compared with data from Newton and Manning (2002a,b). Consequently, our equations may be sufficient to characterize aqueous silica speciation in low silica activity assemblages, at least in the absence of Al. In fluids in equilibrium with aluminosilicate assemblages, our results will provide a useful basis for retrieving the thermodynamic properties of more complex Al–Si species.

In the case of the aqueous Al species, $AlO(OH)^0_{aq}$ and AlO^-_2, the equation of state coefficients reported here are based on the extensive analysis of lower pressure and temperature solubility data by Pokrovskii and Helgeson (1995) revised to be consistent with more recent data for the solubility of corundum referring to high pressures and temperatures (Tropper and Manning, 2007; Wohlers and Manning, 2009).

Finally, the results of the present study were used to constrain a new predictive correlation for the most important

HKF coefficient governing the pressure dependence of the standard partial molal Gibbs free energy of aqueous species. At pressures greater than about 10 kb, the pressure dependence of the free energy is dominated by the coefficient a_1 because $\Delta\overline{G}^0_{P_r\rightarrow P}$ is proportional to $a_1(P - P_r)$. The correlation previously used to estimate values of a_1 based on five monatomic ions (Shock and Helgeson, 1988) is not appropriate for complex aqueous species at high pressures. A new correlation was established using results of the regression calculations in the present study, and those from an independent analysis of volumes and compressibilities in the literature (Plyasunov and Shock, 2001). The results show that the values of the coefficient a_1 for $SiO^0_{2,aq}$ and $Si_2O^0_{4,aq}$ are consistent with a wide variety of other neutral and complex species, both inorganic and organic. As a consequence, this result enables prediction of a_1 for complex aqueous species if the standard partial molal volume of the species at 25 °C and 1 bar is known or can be estimated.

Overall, the results of the present study represent a first step forward in the quantitative geochemical prediction of the properties of aqueous species in deep fluids in the Earth. Much more experimental data is needed on the properties of water and dissolved electrolytes, and the solubilities and aqueous speciation of all the chemical elements of interest in the deep Earth. At the same time, intensive efforts are needed in the application of quantum chemical approaches to understanding speciation in high temperature/pressure fluids. The present study provides a theoretical framework for integrating past and future experimental and theoretical studies, with the overall goal of being able to predict water–rock interactions and the role of aqueous fluids in the geochemical cycles of the elements in the deep Earth.

ACKNOWLEDGEMENTS

This research was supported by grants from the Sloan Foundation through the Deep Carbon Observatory (Reservoirs and Fluxes, and Extreme Physics and Chemistry programs). Additional support was provided by grants DOE DE-FG-02-96ER-14616 and NSF EAR 1023865. We thank the Associate Editor Gleb Pokrovski, reviewer David Dolejš, and two anonymous reviewers for their helpful comments on the manuscript. We gratefully acknowledge the help and support of the Johns Hopkins University, the Geophysical Laboratory of the Carnegie Institution of Washington, and the Université Claude Bernard 1 (Lyon), as well as the stimulating environment of the Bistro Martine in Lyon (thank you Martine, Susanna and Annie). We also wish to acknowledge numerous helpful discussions about the meaning and use of the dielectric constant with George Cody, Ron Cohen, Yingwei Fei, Dionysis Foustoukos, Chris Glein, Bob Hazen, Rus Hemley, Bjorn Mysen and Craig Schiffries (CIW), Dennis Bird (Stanford), Giulia Galli, Ding Pan and Leonardo Spanu (UC Davis), Mark Ghiorso (OFM Research), Craig Manning (UCLA), and Everett Shock (ASU). The senior author would particularly like to acknowledge the singular stimulus for this project provided by Isabelle Daniel (Université Claude Bernard 1 & ENS-CNRS, Lyon) who first suggested that he calculate the dielectric constant at high pressure and who, together with Sébastien Facq, carried out pioneering experimental studies of carbonate speciation at extreme pressures thereby establishing a challenge for geochemical theory that we hope we have taken a useful first step towards meeting.

APPENDIX A. SUPPLEMENTARY DATA

Supplementary data associated with this article can be found, in the online version, at http://dx.doi.org/10.1016/j.gca.2013.12.019.

REFERENCES

Abramson E. H. and Brown J. M. (2004) Equation of state of water based on speeds of sound measured in the diamond-anvil cell. *Geochim. Cosmochim. Acta* **68**, 1827–1835.

Amend J. P. and Helgeson H. C. (1997a) Calculation of the standard molal thermodynamic properties of aqueous aqueous biomolecules at elevated temperatures and pressures. 1. L-alpha amino acids. *J. Chem. Soc. Faraday Trans.* **93**, 1927–1941.

Amend J. P. and Helgeson H. C. (1997b) Group additivity equations of state for calculating the standard molal thermodynamic properties of aqueous organic species at elevated temperatures and pressures. *Geochim. Cosmochim. Acta* **61**, 11–46.

Amend J. P., LaRowe D. E., McCollom T. M. and Shock E. L. (2013) The energetics of organic synthesis inside and outside the cell. *Phil. Trans. Roy. Soc. B Biol. Sci.*, 368.

Anderson G. M. (2005) *The Thermodynamics of Natural Systems*. Cambridge University Press, Cambridge, UK.

Anderson G. M. and Burnham C. W. (1965) The solubility of quartz in super-critical water. *Am. J. Sci.* **263**, 494–511.

Anderson G. M., Castet S., Schott J. and Mesmer R. E. (1991) The density model for estimation of thermodynamic parameters of reactions at high temperatures and pressures. *Geochim. Cosmochim. Acta* **55**, 1769–1779.

Becker K. H., Cemiç L. and Langer K. E. O. E. (1983) Solubility of corundum in supercritical water. *Geochim. Cosmochim. Acta* **47**, 1573–1578.

Berman R. G. (1988) Internally-consistent thermodynamic data for minerals in the system Na_2O–K_2O–CaO–MgO–FeO–Fe_2O_3–Al_2O_3–SiO_2–TiO_2–H_2O–CO_2. *J. Petrol.* **29**, 445–522.

Bethke C. M. (1996) *Geochemical Reaction Modeling*. Oxford University Press, New York.

Brodholt J. P. and Wood B. J. (1994) Measurements of the PVT of water to 25 kbars and 1600 °C from synthetic fluid inclusions in corundum. *Geochim. Cosmochim. Acta* **58**, 2143–2148.

Burnham C. W., Holloway J. R. and Davis N. F. (1969) Specific volume of water in the range 1000 to 8900 bars, 20° to 900° C. *American Journal of Science* **267**, 70–95.

Caciagli N. and Manning C. (2003) The solubility of calcite in water at 6–16 kbar and 500–800 °C. *Contrib. Miner. Petrol.* **146**, 275–285.

Chou I.-M., Bassett W. A., Anderson A. J., Mayanovic R. A. and Shang L. (2008) Containment of fluid samples in the hydrothermal diamond-anvil cell without the use of metal gaskets: performance and advantages for in situ analysis. *Rev. Sci. Instrum.* **79**, 115103.

Chou I. M. and Anderson A. J. (2009) Diamond dissolution and the production of methane and other carbon-bearing species in hydrothermal diamond-anvil cells. *Geochim. Cosmochim. Acta* **73**, 6360–6366.

Cogan, H. L. (1958) Ph. D. Dissertation, Yale University.

Crerar D. A. and Anderson G. M. (1971) Solubility and solvation reactions of quartz in dilute hydrothermal solutions. *Chem. Geol.* **8**, 107–122.

Dandurand J.-L. and Schott J. (1987) New data on the solubility of amorphous silica in organic compound-water solutions and a new model for the thermodynamic behavior of aqueous silica in aqueous complex solutions. *J. Solution Chem.* **16**, 237–256.

Deul, H. L. (1984) Ph. D. Dissertation, University of Karlsruhe.

Diakonov I., Pokrovski G., Schott J., Castet S. and Gout R. (1996) An experimental and computational study of sodium–aluminum complexing in crustal fluids. *Geochim. Cosmochim. Acta* **60**, 197–211.

Dick J. M., LaRowe D. E. and Helgeson H. C. (2006) Temperature, pressure, and electrochemical constraints on protein speciation: group additivity calculation of the standard molal thermodynamic properties of ionized unfolded proteins. *Biogeosciences* **3**, 311–336.

Dick J. M. and Shock E. L. (2013) A metastable equilibrium model for the relative abundances of microbial phyla in a hot spring. *PLoS ONE* **8**, e72395.

Dolejš D. (2013) Thermodynamics of aqueous species at high temperatures and pressures: equations of state and transport theory. *Rev. Mineral. Geochem.* **76**, 35–79.

Dolejš D. and Manning C. E. (2010) Thermodynamic model for mineral solubility in aqueous fluids: theory, calibration and application to model fluid-flow systems. *Geofluids* **10**, 20–40.

Ellis A. and McFadden I. (1972) Partial molal volumes of ions in hydrothermal solutions. *Geochim. Cosmochim. Acta* **36**, 413–426.

Facq S., Daniel I. and Sverjensky D. A. (2014) In situ Raman study and thermodynamic model of aqueous carbonate speciation in equilibrium with aragonite under subduction zone conditions. *Geochim. Cosmochim. Acta* http://dx.doi.org/10.1016/j.gca.2014.01.030..

Fernández D. P., Goodwin A. R. H., Lemmon E. W., Sengers J. M. H. L. and Williams R. C. (1997) A formulation for the static permittivity of water and steam at temperatures from 238 K to 873 K at pressures up to 1200 MPa, including derivatives and Debye–Huckel coefficients. *J. Phys. Chem. Ref. Data* **26**, 1125–1166.

Fernández D. P., Mulev Y., Goodwin A. R. H. and Sengers J. M. H. L. (1995) A database for the static dielectric-constant of water and steam. *J. Phys. Chem. Ref. Data* **24**, 33–69.

Franck E. U., Rosenzweig S. and Christoforakos M. (1990) Calculation of the dielectric-constant of water to 1000-degrees-C and very high-pressures. *Ber. Bunsenges. Phys. Chem.* **94**, 199–203.

Frantz J. D., Dubessy J. and Mysen B. O. (1994) Ion-pairing in aqueous $MgSO_4$ solutions along an isochore to 500 °C and 11 kbar using Raman spectroscopy in conjunction with the diamond-anvil cell. *Chem. Geol.* **116**, 181–188.

Haar L., Gallapher J. S. and Kell G. S. (1984) *NBS/NRC Steam Tables*. Hemisphere Pub. Co..

Heger K., Uematsu M. and Franck E. U. (1980) The static dielectric constant of water at high pressures and temperatures to 500 MPa and 550 °C. *Ber. Bunsenges. Phys. Chem.* **84**, 758–762.

Helgeson H. C. (1964) *Complexing and hydrothermal ore deposits*. MacMillan Co., New York.

Helgeson H. C. (1970). A chemical and thermodynamic model of ore deposition in hydrothermal systems. In: *Mineralogical Society of America Special Paper, Fiftieth Anniv. Symp.*, Vol. 3 (ed. B. A. Morgan) pp. 155–186.

Helgeson H. C. (1979) Mass transfer among minerals and hydrothermal solutions. In *Geochemistry of Hydrothermal Ore Deposits* (ed. H. L. Barnes). Holt, Rhinehart, and Winston.

Helgeson H. C., Delaney J. M., Nesbitt H. W. and Bird D. K. (1978) Summary and critique of the thermodynamic properties of rock-forming minerals. *Am. J. Sci.* **278A**, 229.

Helgeson H. C. and Kirkham D. H. (1974a) Theoretical prediction of the thermodynamic behavior of aqueous electrolytes at high pressures and temperatures: I. Summary of the thermodynamic/electrostatic properties of the solvent. *Am. J. Sci.* **274**, 1089–1198.

Helgeson H. C. and Kirkham D. H. (1974b) Theoretical prediction of the thermodynamic behavior of aqueous electrolytes at high pressures and temperatures: II. Debye–Hückel parameters for activity coefficients and relative partial molal properties. *Am. J. Sci.* **274**, 1199–1261.

Helgeson H. C. and Kirkham D. H. (1976) Theoretical prediction of the thermodynamic properties of aqueous electrolytes at high pressures and temperatures. III. Equation of state for aqueous species at infinite dilution. *Am. J. Sci.* **276**, 97–240.

Helgeson H. C., Kirkham D. H. and Flowers G. C. (1981) Theoretical prediction of the thermodynamic behavior of aqueous electrolytes at high pressures and temperatures. IV. Calculation of activity coefficients, osmotic coefficients, and apparent molal and standard and relative partial molal properties to 5 kb and 600 °C. *Am. J. Sci.* **281**, 1241–1516.

Hemley J. J., Montoya J. W., Marinenko J. W. and Luce R. W. (1980) Equilibria in the system Al_2O_3–SiO_2–H_2O and some general implications for alteration/mineralization processes. *Econ. Geol.* **75**, 210–228.

Hemley J. J., Montoya J. W., Shaw D. R. and Luce R. W. (1977) Mineral equilibria in the MgO–SiO_2–H_2O sytem: II talc–anigorite–forsterite–anthophyllite–enstatite stability relations and some geologic implications in the system. *Am. J. Sci.* **277**, 353–383.

Hnedkovsky L., Majer V. and Wood R. H. (1995) Volumes and heat capacities of H_3BO_3(aq) at temperatures from 298.15 K to 705 K and at pressures to 35 MPa. *J. Chem. Thermodyn.* **27**, 801–814.

Ho P. C. and Palmer D. A. (1997) Ion association of dilute aqueous potassium chloride and potassium hydroxide solutions to 600 °C and 300 MPa determined by electrical conductance measurements. *Geochim. Cosmochim. Acta* **61**, 3027–3040.

Holland T. J. B. and Powell R. (2011) An improved and extended internally consistent thermodynamic dataset for phases of petrological interest, involving a new equation of state for solids. *J. Metamorph. Geol.* **29**, 333–383.

Hovey J. K. and Tremaine P. R. (1986) Thermodynamics of aqueous aluminum: standard partial molar heat capacities of Al3+ from 10 to 55 °C. *Geochim. Cosmochim. Acta* **50**, 453–459.

Hunt J. D., Kavner A., Schauble E. A., Snyder D. and Manning C. E. (2011) Polymerization of aqueous silica in H_2O–K_2O solutions at 25–200 °C and 1 bar to 20 kbar. *Chem. Geol.* **283**, 161–170.

Hunt J. D. and Manning C. E. (2012) A thermodynamic model for the system near the upper critical end point based on quartz solubility experiments at 500–1100 °C and 5–20 kbar. *Geochim. Cosmochim. Acta* **86**, 196–213.

Johnson J. W. and Norton D. (1991) Critical phenomena in hydrothermal systems: state, thermodynamic, electrostatic, and transport properties of H_2O in the critical region. *Am. J. Sci.* **291**, 541–648.

Johnson J. W., Oelkers E. H. and Helgeson H. C. (1992) SUPCRT92: a software package for calculating the standard molal thermodynamic properties of minerals, gases, aqueous species, and reactions from 1 to 5000 bars and 0 to 1000 °C. *Comput. Geosci.* **18**, 899–947.

LaRowe D. E. and Helgeson H. C. (2006) Biomolecules in hydrothermal systems: calculation of the standard molal thermodynamic properties of nucleic-acid bases, nucleosides, and nucleotides at elevated temperatures and pressures. *Geochim. Cosmochim. Acta* **70**, 4680–4724.

Larrieu T. L. and Ayers J. C. (1997) Measurements of the pressure–volume–temperature properties of fluids to 20 kbar and

1000 °C: a new approach demonstrated on H_2O. *Geochim. Cosmochim. Acta* **61**, 3121–3134.

Manning C. E. (1994) The solubility of quartz in H_2O in the lower crust and upper-mantle. *Geochim. Cosmochim. Acta* **58**, 4831–4839.

Manning C. E. (2004) The chemistry of subduction-zone fluids. *Earth Planet. Sci. Lett.* **223**, 1–16.

Manning C. E. (2013) Thermodynamic modeling of fluid–rock Interaction at mid-crustal to upper-mantle conditions. *Rev. Mineral. Geochem.* **76**, 135–164.

Manning C. E., Antignano A. and Lin H. A. (2010) Premelting polymerization of crustal and mantle fluids, as indicated by the solubility of albite + paragonite + quartz in H_2O at 1 GPa and 350–620 °C. *Earth Planet. Sci. Lett.* **292**, 325–336.

Manning C. E., Shock E. L. and Sverjensky D. A. (2013) The chemistry of carbon in aqueous fluids at crustal and upper-mantle conditions: experimental and theoretical constraints. In *Carbon in Earth* (eds. R. M. Hazen, J. A. Baross and A. P. Jones). Mineralogical Society of America.

Mantegazzi D., Sanchez-Valle C. and Driesner T. (2013) Thermodynamic properties of aqueous NaCl solutions to 1073°K and 4.5 GPa, and implications for dehydration reactions in subducting slabs. *Geochim. Cosmochim. Acta* **121**, 263–290.

Mantegazzi D., Sanchez-Valle C., Reusser E. and Driesner T. (2012) Thermodynamic properties of aqueous sodium sulfate solutions to 773 K and 3 GPa derived from acoustic velocity measurements in the diamond anvil cell. *J. Chem. Phys.* **137**, 224501–224512.

Marshall W. L. (2008) Dielectric constant of water discovered to be simple function of density over extreme ranges from –35 to +600°C and to 1200 MPa (12000 Atm.), believed Universal. *Nat. Precedings*. http://dx.doi.org/10.1038/npre.2008.2472.1.

Marshall W. L. and Franck E. U. (1981) Ion product of water substance, 0 °C – 1000 °C, 1–10,000 bars – new international formulation and its background. *J. Phys. Chem. Ref. Data* **10**, 295–304.

Martinez I., Sanchez-Valle C., Daniel I. and Reynard B. (2004) High-pressure and high-temperature Raman spectroscopy of carbonate ions in aqueous solution. *Chem. Geol.* **207**, 47–58.

McCollom T. M. and Shock E. L. (1998) Fluid–rock interactions in the lower oceanic crust: thermodynamic models of hydrothermal alteration. *J. Geophys. Res.* **103**, 547–575.

McKenzie W. F. and Helgeson H. C. (1984) Estimation of the dielectric constant of H_2O from experimental solubilities of quartz and the calculation of the thermodynamic properties of aqueous species to 900 °C at 2 kb. *Geochim. Cosmochim. Acta* **48**, 2167–2177.

Mesmer R. E., Baes C. F. and Sweeton F. H. (1972) Acidity measurements at elevated temperatures. VI. Boric acid equilibriums. *Inorg. Chem.* **11**, 537–543.

Mibe K., Chou I. M. and Bassett W. A. (2008) In situ Raman spectroscopic investigation of the structure of subduction-zone fluids. *J. Geophys. Res.* **113**, B04208.

Morey G. W., Fournier R. O. and Rowe J. J. (1962) The solubility of quartz in water in the temperature interval from 25 to 300 °C. *Geochim. Cosmochim. Acta* **26**, 1029–1043.

Mysen B. O. (2009) Solution mechanisms of silicate in aqueous fluid and H_2O in coexisting silicate melts determined in-situ at high pressure and high temperature. *Geochim. Cosmochim. Acta* **73**, 5748–5763.

Mysen B. O. (2010) Speciation and mixing behavior of silica-saturated aqueous fluid at high temperature and pressure. *Am. Miner.* **95**, 1807–1816.

Mysen B. O., Tomita T., Ohtani E. and Suzuki A. (2013a) Speciation of and D/H partitioning between fluids and melts in silicate – D–O–H–C–N systems determined *in situ* at upper mantle temperatures, pressures, and redox conditions. *Am. Miner.* (in press). http://dx.doi.org/10.2138/am.2014.4575.

Mysen, B., Mibe, K., Chou, I. M., and Bassett, W., (2013b). Structure and equilibria among silicate species in aqueous fluids in the upper mantle: Experimental SiO_2–H_2O and MgO–SiO_2–H_2O data recorded in situ to 900°C and 5.4 GPa. *J. Geophys. Res-Sol. Ea.*

Mysen B. O. and Yamashita S. (2010) Speciation of reduced C–O–H volatiles in coexisting fluids and silicate melts determined in-situ to similar to 1.4 GPa and 800 degrees C. *Geochim. Cosmochim. Acta* **74**, 4577–4588.

Newton R. C. and Manning C. E. (2000) Quartz solubility in H_2O–NaCl and H_2O–CO_2 solutions at deep crust-upper mantle pressures and temperatures: 2–15 kbar and 500–900 degrees C. *Geochim. Cosmochim. Acta* **64**, 2993–3005.

Newton R. C. and Manning C. E. (2002a) Activity coefficient and polymerization of aqueous silica based on high-PT solubility measurements. *Geochim. Cosmochim. Acta* **66**, A551.

Newton R. C. and Manning C. E. (2002b) Solubility of enstatite + forsterite in H_2O at deep crust/upper mantle conditions: 4 to 15 kbar and 700 to 900 °C. *Geochim. Cosmochim. Acta* **66**, 4165–4176.

Newton R. C. and Manning C. E. (2003) Activity coefficient and polymerization of aqueous silica at 800 degrees C, 12 kbar, from solubility measurements on SiO_2-buffering mineral assemblages. *Contrib. Miner. Petrol.* **146**, 135–143.

Newton R. C. and Manning C. E. (2008) Thermodynamics of SiO_2–H_2O fluid near the upper critical end point from quartz solubility measurements at 10 kbar. *Earth Planet. Sci. Lett.* **274**, 241–249.

Newton R. C. and Manning C. E. (2009) Hydration state and activity of aqueous silica in H_2O–CO_2 fluids at high pressure and temperature. *Am. Miner.* **94**, 1287–1290.

Newton R. C., Manning C. E., Hanchar J. M. and Colasanti C. V. (2010) Free energy of formation of zircon based on solubility measurements at high temperature and pressure. *Am. Miner.* **95**, 52–58.

Palmer D. A. and Wesolowski D. J. (1992) Aluminum speciation and equilibria in aqueous solution: II. The solubility of gibbsite in acidic sodium chloride solutions from 30 to 70 °C. *Geochim. Cosmochim. Acta* **56**, 1093–1111.

Pan D., Spanu L., Harrison B., Sverjensky D. A. and Galli G. (2013) The dielectric constant of water under extreme conditions and transport of carbonates in the deep Earth. *Proc. Nat. Acad. Sci.* **110**, 6646–6650.

Petitgirard S., Daniel I., Dabin Y., Cardon H., Tucoulou R. and Susini J. (2009) A diamond anvil cell for x-ray fluorescence measurements of trace elements in fluids at high pressure and high temperature. *Rev. Sci. Instrum.* **80**, 1–5.

Pitzer K. S. (1983) Dielectric constant of water at very high temperature and pressure. *Proc. Natl. Acad. Sci.* **80**, 4575–4576.

Plyasunov A. V. and Shock E. L. (2001) Correlation strategy for determining the parameters of the revised Helgeson–Kirkham–Flowers model for aqueous nonelectrolytes. *Geochim. Cosmochim. Acta* **65**, 3879–3900.

Pokrovski G. S., Borisova A. Y. and Bychkov A. Y. (2013) Speciation and transport of metals and metalloids in geological vapors. *Rev. Mineral. Geochem.* **76**, 165–218.

Pokrovski G. S. and Dubrovinsky L. S. (2011) The S_3^- ion is stable in geological fluids at elevated temperatures and pressures. *Science* **331**, 1052–1054.

Pokrovskii V. A. and Helgeson H. C. (1995) Thermodynamic properties of aqueous species and the solubilities of minerals at high pressures and temperatures: the system Al_2O_3–H_2O–NaCl. *Am. J. Sci.* **295**, 1255–1342.

Rimstidt J. D. (1997) Quartz solubility at low temperatures. *Geochim. Cosmochim. Acta* **61**, 2553–2558.

Robie R. A. and Hemingway B. S. (1995) Thermodynamic properties of minerals and related substances at 298.15 K and 1 bar (10^5 Pascals) pressure and at higher temperatures. *U.S. Geol. Survey Bull.* **2131**, 461.

Sanchez-Valle C. (2013) Structure and thermodynamics of subduction zone fluids from spectroscopic studies. *Rev. Mineral. Geochem.* **76**, 265–309.

Shock E. L. (1992) Stability of peptides in high temperature aqueous solutions. *Geochim. Cosmochim. Acta* **56**, 3481–3491.

Shock E. L. (1993) Hydrothermal dehydration of aqueous organic compounds. *Geochim. Cosmochim. Acta* **57**, 3341–3349.

Shock E. L. and Canovas P. (2010) The potential for abiotic organic synthesis and biosynthesis at seafloor hydrothermal systems. *Geofluids* **10**, 161–192.

Shock E. L. and Helgeson H. C. (1988) Calculation of the thermodynamic and transport properties of aqueous species at high pressures and temperatures: correlation algorithms for ionic aqueous species and equation of state predictions to 5 kb and 1000 °C. *Geochim. Cosmochim. Acta* **52**, 2009–2036.

Shock E. L. and Helgeson H. C. (1990) Calculation of the thermodynamic and transport properties of aqueous species at high pressures and temperatures: standard partial molal properties of organic species. *Geochim. Cosmochim. Acta* **54**, 915–945.

Shock E. L., Helgeson H. C. and Sverjensky D. A. (1989) Calculation of the thermodynamic and transport properties of aqueous species at high pressures and temperatures: standard partial molal properties of inorganic neutral species. *Geochim. Cosmochim. Acta* **53**, 2157–2184.

Shock E. L., Oelkers E. H., Johnson J. W., Sverjensky D. A. and Helgeson H. C. (1992) Calculation of the thermodynamic and transport properties of aqueous species at high pressures and temperatures: effective electrostatic radii to 1000 °C and 5 kb. *Faraday Soc. Trans.* **88**, 803–826.

Shock E. L., Sassani D. C., Willis M. and Sverjensky D. A. (1997) Inorganic species in geologic fluids: correlations among standard molal thermodynamic properties of aqueous ions and hydroxide complexes. *Geochim. Cosmochim. Acta* **61**, 907–950.

Sjoberg S. (1996) Silica in aqueous environments. *J. Non-Cryst. Solids* **196**, 51–57.

Spiekermann G., Steele-MacInnis M., Kowalski P. M., Schmidt C. and Jahn S. (2012) Vibrational mode frequencies of H_4SiO_4, D_4SiO_4, $H_6Si_2O_7$, and $H_6Si_3O_9$ in aqueous environment, obtained from ab initio molecular dynamics. *J. Chem. Phys.* **137**, 164506–164511.

Sverjensky D. A. (1987) The role of migrating oil-field brines in the formation of sediment-hosted Cu-rich deposits. *Econ. Geol.* **82**, 1130–1141.

Sverjensky D. A., Shock E. L. and Helgeson H. C. (1997) Prediction of the thermodynamic properties of aqueous metal complexes to 1,000 °C and 5.0 kb. *Geochim. Cosmochim. Acta* **61**, 1359–1412.

Tagirov B. and Schott J. (2001) Aluminum speciation in crustal fluids revisited. *Geochim. Cosmochim. Acta* **65**, 3965–3992.

Tagirov B., Schott J., Harrichoury J.-C. and Escalier J. (2004) Experimental study of the stability of aluminate–borate complexes in hydrothermal solutions. *Geochim. Cosmochim. Acta* **68**, 1333–1345.

Tanger J. C. and Helgeson H. C. (1988) Calculation of the thermodynamic and transport properties of aqueous species at high pressures and temperatures: revised equations of state for the standard partial molal properties of ions and electrolytes. *Am. J. Sci.* **288**, 19–98.

Tropper P. and Manning C. E. (2007) The solubility of corundum in H_2O at high pressure and temperature and its implications for Al mobility in the deep crust and upper mantle. *Chem. Geol.* **240**, 54–60.

Wagner W. and Pruß A. (2002) The IAPWS formulation 1995 for the thermodynamic properties of ordinary water substance for general and scientific use. *J. Phys. Chem. Ref. Data* **31**, 387–535.

Walther J. V. and Helgeson H. C. (1977) Calculation of the thermodynamic properties of aqueous silica and the solubility of quartz and its polymorphs at high pressures and temperatures. *Am. J. Sci.* **277**, 1315–1351.

Walther J. V. and Orville P. M. (1983) The extraction-quench technique for determination of the thermodynamic properties of solute complexes: application to quartz solubility in fluid mixtures. *Am. Miner.* **68**, 731–741.

Ward G. K. and Millero F. J. (1974) The effect of pressure on the ionization of boric acid in aqueous solutions from molal-volume data. *J. Solut. Chem.* **3**, 417–430.

Wasserman E., Wood B. J. and Brodholt J. P. (1995) The static dielectric constant of water at pressures up to 20 khar and temperatures to 1273 K: experiment, simulations, and empirical equations. *Geochim. Cosmochim. Acta* **59**, 1–6.

Weill D. F. and Fyfe W. S. (1964) The solubility of quartz in H_2O in the range 1000–4000 bars and 400–550 °C. *Geochim. Cosmochim. Acta* **28**, 1243–1255.

Wesolowski D. J. (1992) Aluminum speciation and equilibria in aqueous solution: I. The solubility of gibbsite in the system Na–K–Cl–OH–Al(OH)4 from 0 to 100 °C. *Geochim. Cosmochim. Acta* **56**, 1065–1091.

Withers A. C., Kohn S. C., Brooker R. A. and Wood B. J. (2000) A new method for determining the P–V–T properties of high-density H_2O using NMR: results at 1.4–4.0 GPa and 700–1100 degrees C. *Geochim. Cosmochim. Acta* **64**, 1051–1057.

Wohlers A. and Manning C. E. (2009) Solubility of corundum in aqueous KOH solutions at 700 °C and 1 GPa. *Chem. Geol.* **262**, 310–317.

Wohlers A., Manning C. E. and Thompson A. B. (2011) Experimental investigation of the solubility of albite and jadeite in H_2O, with paragonite + quartz at 500 and 600 °C, and 1–2.25 GPa. *Geochim. Cosmochim. Acta* **75**, 2924–2939.

Zhang Y. G. and Frantz J. D. (2000) Enstatite-forsterite-water equilibria at elevated temperatures and pressures. *Am. Miner.* **85**, 918–925.

Zhang C. and Duan Z. (2009) A model for C–O–H fluid in the Earth's mantle. *Geochim. Cosmochim. Acta* **73**, 2089–2102.

Zhang Z. and Duan Z. (2005) Prediction of the PVT properties of water over wide range of temperatures and pressures from molecular dynamics simulation. *Phys. Earth Planet. Inter.* **149**, 335–354.

Zhu C. and Anderson G. M. (2002) *Environmental Applications of Geochemical Modeling*. Cambridge, Cambridge.

Zotov N. and Keppler H. (2000) In-situ Raman spectra of dissolved silica species in aqueous fluids to 900 °C and 14 kbar. *Am. Miner.* **85**, 600–604.

Zotov N. and Keppler H. (2002) Silica speciation in aqueous fluids at high pressures and high temperatures. *Chem. Geol.* **184**, 71–82.

Associate editor: Gleb S. Pokrovski